Journal of *Marine Science and Engineering*

MDPI

Article

Quantifying Mechanisms Responsible for Extreme Coastal Water Levels and Flooding during Severe Tropical Cyclone Harold in Tonga, Southwest Pacific

Moleni Tu'uholoaki [1,2,*], Antonio Espejo [3], Moritz Wandres [3], Awnesh Singh [1], Herve Damlamian [3] and Zulfikar Begg [3]

1 Pacific Centre for Environment and Sustainable Development, The University of the South Pacific, Suva, Fiji; awnesh.singh@usp.ac.fj
2 Tonga Meteorological Service, Nuku'alofa, Tonga
3 Geoscience, Energy and Maritime Division, Pacific Community, Suva, Fiji; antonioh@spc.int (A.E.); moritzw@spc.int (M.W.); herveda@spc.int (H.D.); zulfikarb@spc.int (Z.B.)
* Correspondence: s11182388@student.usp.ac.fj or molenit@gmail.com

Abstract: The South Pacific region is characterised by steep shelves and fringing coral reef islands. The lack of wide continental shelves that can dissipate waves makes Pacific Island countries vulnerable to large waves that can enhance extreme total water levels triggered by tropical cyclones (TCs). In this study, hindcasts of the waves and storm surge induced by severe TC Harold in 2020 on Tongatapu, Tonga's capital island, were examined using the state-of-the-art hydrodynamic and wave models ADCIRC and SWAN. The contributions of winds, atmospheric pressure, waves, and wave-radiation-stress-induced setup to extreme total water levels were analysed by running the models separately and two-way coupled. The atmospheric pressure deficit contributed uniformly to the total water levels (~25%), while the wind surge was prominent over the shallow shelf (more than 75%). Wave setup became significant at locations with narrow fringing reefs on the western side (more than 75%). Tides were dominant on the leeward coasts of the island (50–75%). Storm surge obtained from the coupled run without tide was comparable with the observation. The wave contribution to extreme total water levels and inundation was analysed using XBEACH in non-hydrostatic mode. The model (XBEACH) was able to reproduce coastal inundation when compared to the observed satellite imagery after the event on a particular coastal segment severely impacted by coastal flooding induced by TC Harold. The coupled ADCIRC+SWAN underestimated total water levels nearshore on the reef flat and consequently inundation extent as infragravity waves and swash motion are not resolved by these models. The suite of models (ADCIRC+SWAN+XBEACH) used in this study can be used to support the Tonga Meteorological Service Tropical Cyclone Early Warning System.

Keywords: storm surge; ADCIRC; SWAN; XBEACH; Tonga; flooding; tropical cyclone Harold

Citation: Tu'uholoaki, M.; Espejo, A.; Wandres, M.; Singh, A.; Damlamian, H.; Begg, Z. Quantifying Mechanisms Responsible for Extreme Coastal Water Levels and Flooding during Severe Tropical Cyclone Harold in Tonga, Southwest Pacific. *J. Mar. Sci. Eng.* **2023**, *11*, 1217. https://doi.org/10.3390/jmse11061217

Academic Editor: Alfredo L. Aretxabaleta

Received: 10 May 2023
Revised: 25 May 2023
Accepted: 26 May 2023
Published: 13 June 2023

1. Introduction

Tropical cyclones (TCs) account for ~76% of natural disasters affecting Pacific Island countries [1]. Although associated rainfall and destructive winds continue wreaking havoc on these islands periodically [2,3], the induced storm surges[1] are the world's most deadly and destructive natural hazard [4]. Most Pacific islands are low-lying reef-fronted islands [5,6] located in a region where sea level is rising at an unprecedented rate [7–9] of currently 3.5 to 5 mm/yr in most of the exclusive economic zones in the region [10,11], larger than the global average of 3.1 mm/yr [12]. Furthermore, recent studies indicate that the intensity and frequency of severe TCs in the central South Pacific are increasing [13–15]. With the majority of the South Pacific's population residing near the coastline [16], and critical infrastructures located within its vicinity [17], the projected increase in intense TCs [18,19]

and sea levels will significantly heighten the risk to coastal flooding (see [20];which depends on various ocean and atmospheric forcings, such as astronomical tides, waves, winds, as well as local bathymetry and topography which drives the inherent nearshore processes). In this context, it is necessary to strengthen our disaster risk knowledge associated with TC-induced coastal flooding which directly support enhanced early warning system and the provision of actionable information to inform emergency preparedness and long-term planning.

Because of the hazardous effect and catastrophic damage of coastal flooding to communities, the World Meteorological Organisation (WMO), headquartered in Geneva, Switzerland, established the Storm Surge Watch Scheme (SSWS) in 2008 to support the National Meteorological and Hydrological Services (NMHS) in providing storm surge forecasting in real time [21]. Recently, the WMO Regional Specialised Meteorological Centre (RSMC) in Fiji established a storm surge forecasting system for the member countries under its responsibility using the Japanese Meteorological Agency (JMA) storm surge model. The aim was to develop an integrated inundation forecasting system. However, storm surge is only one of the processes driving coastal flooding in the Pacific island region. In turn, storm surge driven inundation forecast, without proper consideration for waves and inherent nearshore processes, would in most cases wrongly inform emergency response. In addition, a group of coastal wave modellers and scientists from around the world has recently formed a working group named UFORIC (Understanding Flooding of Reef-lined Coasts; [22]) with a working plan to meet regularly to address the issues facing coral-reef lined shorelines in terms of data and tools. The main aim is to have sufficient data and efficient tools to develop a Coastal Flood Early Warning System in the short term and provide long-term projections based on future global warming scenarios to help plan and mitigate coastal risks.

Most studies focus on extreme waves, storm surges, and coastal inundations in large continental shelf regions with mild slopes, in which the wind setup plays a major role in coastal inundations [23,24]. In contrast, in reef-fronted or volcanic islands where shelves are steep with narrow fringing reefs, wave setup and infragravity waves (e.g., [22,25–27]), and inverted barometer effect [27] play a major role in driving coastal inundation. Apart from countries with mild-slope continental shelves, any storm surge forecasting system/hindcast study that does not include these physical processes (e.g., wave setup) might not be providing accurate warnings/results of imminent/past coastal inundation [21]; therefore, in the tropical Pacific, where fringing and barrier coral reefs dominate the coastlines, it is vital to evaluate the performance of state-of-the-art modelling tools and their ability to account for the combined effects of tides, storm surges, and waves in the South Pacific.

Because of the lack of relevant studies in this region, very little is known about the hydrodynamics and inherent non-linear nearshore processes driving coastal inundation in most of these countries. This scarcity of published materials is compounded by a lack of in situ observational data, especially on wave measurements and nearshore wave climate, island topography and high-resolution bathymetric data, local sea level, and the absence of a regional and local coupled storm surge and wave models [22]. The Climate and Oceans Support Programme in the Pacific (COSPPac) has installed tide gauges in 12 Pacific countries for over 20 years but limited them only to the main islands of these countries, making it challenging to quantify the impact of sea levels, tides, and storm surges on the remote islands. The persistent threat of rising sea levels and catastrophic tropical cyclones presents an ongoing difficulty for nations to create policies and make decisions based on reliable information.

Therefore, it is relevant to explore the suitability of state-of-the-art wave and circulation models, such as ADCIRC (advanced circulation; [28]) and SWAN (simulating waves nearshore; [29]), to reproduce past flooding events and evaluate their performance to be used operationally forIcoastal inundation forecasting. Although ADCIRC and SWAN are often coupled and widely used in the Northern Hemisphere for research and operational forecasting (e.g., [30–33]), to the best of our knowledge, the coupled models have never been tested or investigated for modelling TC inundation hazardin the South Pacific region.

Previous studies indicate that this coupled model suite is very useful for computing coastal inundation even in data-sparse regions [33], such as the South Pacific, and can offer more knowledge about the hydrodynamics nearshore during the passage of a TC [34].

Storm surge and waves depend on the topographic and bathymetric features, and characteristics of TCs (intensity, radius of maximum winds, forward speed, and angle of landfall). Additionally, the timing of tides can greatly modulate the storm tide[2] and wave energy dissipation and, in turn, the maximum total water level nearshore (e.g., [2,25,26,35–37]). Therefore, various approaches to tuning model parameters to accurately predict waves, tides and storm surges, such as varying bottom frictions, experimenting with different drag formulations coefficients, and different atmospheric forcings [30,38], need to be conducted. Here, as a first step towards developing a TC driven coastal inundation forecasting and early warning system for Tonga, we focus on using a coupled model and uncoupled model to examine the relative contributions of tidal and atmospheric model forcings (tides, inverted barometer response to atmospheric pressure, wind-induced surface stresses, and wind wave setup) on water levels.

Atmospheric forcing is the main storm surge driver [39,40] represented in the form of winds and barometric pressure fields. There are several approaches to producing TC wind fields for storm surge modelling: parametric wind models (e.g., [41,42]), full-based atmospheric physics models (e.g., Weather Research Forecasting (WRF) Model; [43]) and kinematic analysis (e.g., surface wind analysis system (HWind) by Hurricane Research Division; [44]). Although the kinematic approach, whereby observed data are assimilated into the model winds, may appear to be more accurate when compared with observed data, these wind field data are not widely available for all areas and cause numerous delays in real-time due to prepossessing of a large number of datasets [30].

In addition, the full atmospheric physics model may potentially produce winds that are accurate but at a high computational cost, and hence may not be suitable for operational forecasting in areas with limited resources, such as the case in the South Pacific. The parametric/analytic TC wind models on the other hand have been widely used and resulted in storm surge estimates comparable to observations [40,43,45] and could outdo full atmospheric physics models, such as WRF, given the best possible best track data are available (e.g., [43]). Parametric wind models have been widely used for hindcast and operational forecasting due to their simplicity, low computational cost, and flexibility (e.g., implemented in the NOAA's Parametric Hurricane Modeling (PaHM) system; [46]), and most of them are available in ADCIRC. In this present study, we used the parametric dynamic Holland model (DHM; [30]).

The majority of extreme storm surge events in these remote island countries remain largely undocumented in the scientific literature. For example, the last meteorological case study of a TC event in Tonga was TC Isaac in March 1982 [35] which claimed six lives, which were attributed to drowning. The storm surge crossed the beachfront road of Nuku'alofa (Tonga) at a height of ~0.6 m and inundated low-lying areas for distances up to 1 km inland [47] and caused a storm surge approximately 1.5 m above high tide [48]. Following this disaster, the Japanese Government built a seawall along the shoreline of Nuku'alofa as a mitigation measure. Since TC Isaac, 85 TCs have impacted Tonga; however, few of those were investigated by the scientific community. Recently, TC Harold came to life hovering over the Coral Sea and transcending the Pacific from 2 to 10 April 2020. It reached a category five maximum strength and impacted several Pacific Island countries, including the Solomon Islands, Vanuatu, Fiji, and Tonga, causing widespread damage and loss of life [49]. Extreme waves and storm surge caused widespread coastal inundation in coastal areas of Tongatapu coinciding with the high tide on 9 April 2020 around 7 am local time, leading to major structural damages to buildings, roads and wharves [50] and the cost of the damage amount to USD 111 m [51].

In the present study, we investigate the storm surge and waves generated by TC Harold by using a range of numerical models. Unlike the case studies of Hoeke et al. [36], Merrifield et al. [52], Wandres et al. [53], and Hoeke et al. [54] in the Pacific, which focused

on events triggered by distant–source weather systems (i.e., mid-latitude low-pressure systems and distant TCs), TC Harold made a direct hit ("direct hit", defined when the eye is within one degree of the land; see [55]) on Nuku'alofa, the capital of Tonga and triggered an extreme water level that caused coastal inundation and damage in the coastal areas of Tongatapu, the main island of Tonga. In particular, we investigate the performance of the coupled ADCIRC + SWAN model and the uncoupled ADCIRC model in the hindcast of the storm surges and total water levels, as well as the relative contributions of the tide, wave setup, wind surge, and atmospheric pressure to the total water levels associated with the severe TC Harold. The phase resolving wave and hydrodynamic XBEACH model [56] is also implemented in nonhydrostatic mode on a segment of the coastline to examine the contribution of wave setup and infragravity waves to the total water levels, and coastal inundation associated with TC Harold. This was done, as ADCIRC and SWAN cannot resolve the full runup, to demonstrate a potential TC inundation forecast system and flood forecasting early warning system (EWS) based on ADCIRC, SWAN, and the XBEACH model.

The rest of the paper is organized as follows: Section 2 outlines the method and data used in this study; the results and discussions are presented in Section 3; and Section 4 provides the conclusions of this study.

2. Method and Data

2.1. Study Site

Tonga is located in the South Pacific Ocean and to the southeast of Fiji or halfway between New Zealand and Hawaii. There are three main island groups in Tonga: Vava'u, Ha'apai and Tongatapu. Tongatapu, the main island of Tonga, is part of the largest and southernmost group (Figure 1a,b).

Nuku'alofa is the capital of Tonga, located on the northern shore of Tongatapu. The capital is home to two-thirds of the population, main infrastructures, trades, businesses, and government offices; hence, it is a critical area for the economy and development of the country. Other capital cities are Neiafu in Vava'u and Pangai in Ha'apai.

Tongatapu is in a shallow narrow strip adjacent to deep ocean water, especially to the immediate east where the Tonga Trench lies (i.e., ~200 km east of Nuku'alofa; see Figure 1b). Tongatapu is surrounded by a chain of islands (see Figure 1a,b) with swampy and extensive reefs and lagoons to the north, and narrow fringing coral reefs to the rest. To the eastern side lies the Tonga Trench (see the blue narrow strip east of Tonga in Figure 1b), with a depth up to 10,000 m below sea level, and the western side is a large plateau, around 3000 m depth below sea level, with Fiji lying to the northwest. Hence, Tongatapu is located in a shallow region influenced by strong currents with eddies trapping energy and dissipating long-wave phenomena and tides due to the abrupt changes in the depth between the eastern and western sides [57].

Climatologically, Nuku'alofa is expected to experience ~2.6 TCs a year. The majority of TCs entering the Tonga region are from the northwest, reaching maximum intensity as they track closer to Nuku'alofa [55]. Theoretically, this northwest approach of TCs directs the body of water at the left-forward quadrant of TCs, where winds are strongest and consequently storm surges are maximum, towards Nuku'alofa.

The wave climate in Nuku'alofa is dominated by easterly waves generated by the southeast trade winds. The annual mean significant wave height (H_s) is 1.30 m, the annual mean direction (θ_p) is 61°, and the annual mean peak period (T_p) is 10.33 s [10]. Approximately 70% of the largest wave events between 1973 and 2013 were associated with TCs approaching Nuku'alofa from the northwest [58]. A parametric wave model study in the Southwest Pacific showed that the latitude band (15–25° S) where Tonga lies produced the largest extreme significant wave heights triggered by TCs in this region, with a maximum height of 11.25 m for a return period of 10 years and 15 m for a return period of 50 years [59].

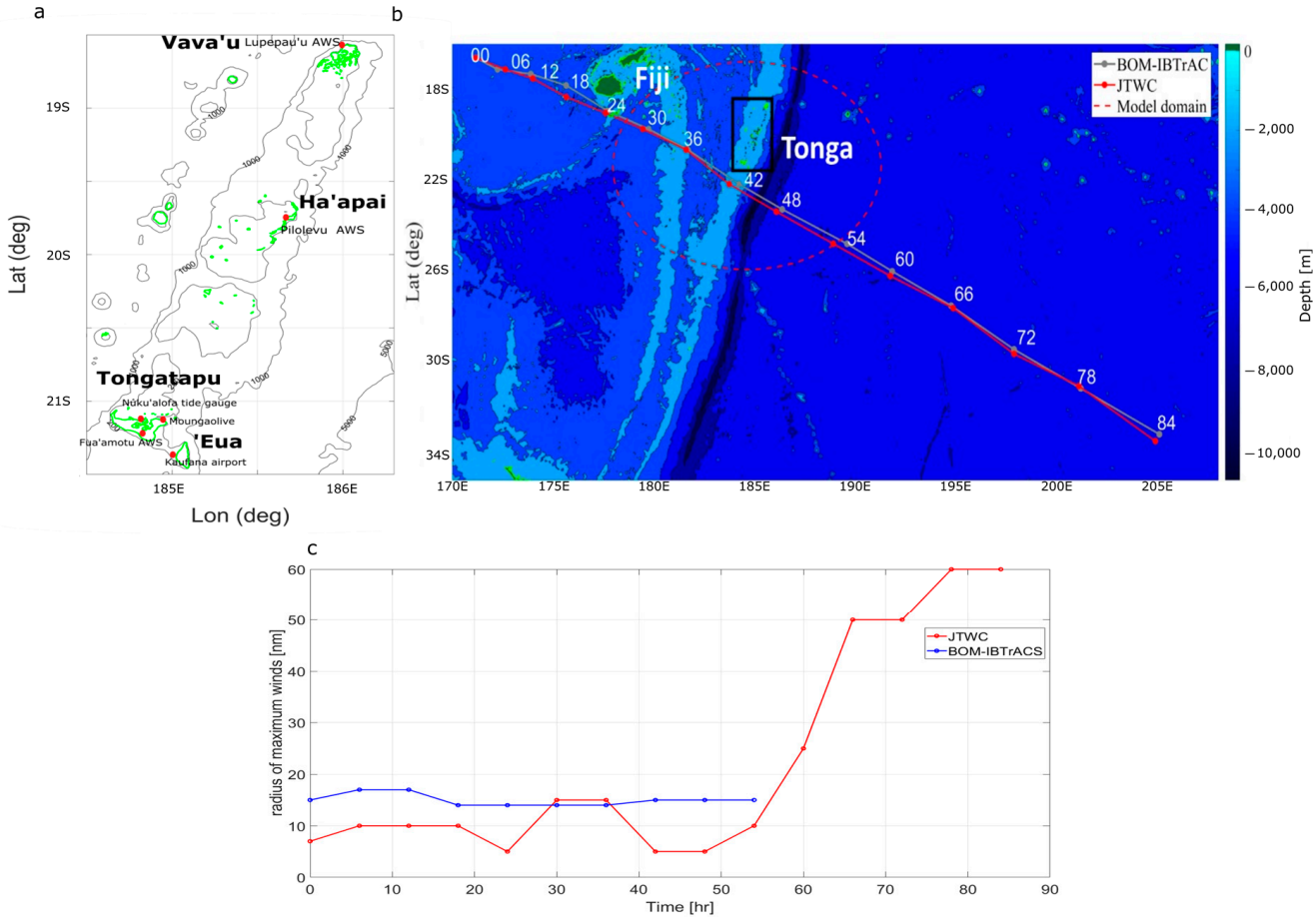

Figure 1. (**a**) Map of Tonga with the main islands (in bold), and observation sites labelled and represented by red dots. The 200 m and 1000 m bathymetric contours around the main islands are showing the location of the island shelves. Coastlines are shown in green coloured lines. (**b**) Bathymetry map of the southwest Pacific region, illustrating the location of Fiji and Tonga. Superimposed is the best track data for TC Harold from the Bureau of Meteorology (in brown) and the Joint Typhoon Warning Centre (in red), with the numbers indicating time (in hours) from 00h00 UTC, 7 April 2022 (00 h) to 12h00 UTC, 10 April 2020 (84 h). The study area (denoted by a dashed red line) is centred on Nuku'alofa. The Tonga trench can be identified with depths greater than 8000 m lying east of Tonga. (**c**) The radius of maximum winds (in nautical miles) for TC Harold from the Bureau of Meteorology (in blue) and the Joint Typhoon Warning Centre (in red).

2.2. Met-Ocean Measurements

The readings from the Nuku'alofa tide gauge station (21.13° S, 184.5° E), which is under the COSPPac, (http://www.bom.gov.au/pacificsealevel/; accessed 20 June 2022) funded by the Australian Government and located at the Vuna wharf in Nuku'alofa, were obtained to validate model output in this study. This station provides hourly sea surface level pressures (hPa), surface winds (m/s), sea levels (m), and sea surface temperature (°C).

In addition, the readings from five automatic weather stations (AWS) from the observation network of the Tonga Meteorological Service archived at the Neon system of the National Institute of Water and Atmosphere (NIWA; https://neon.niwa.co.nz//logon.aspx; accessed 19 May 2022) were used to validate the model winds and pressures. These AWS cover the Lupepau'u airport in Vava'u, Pilolevu airport in Ha'apai, Mo'unga'olive, and Fua'amotu airport in Tongatapu, and Kaufana airport in 'Eua (see Figure 1a). Most of them are located inland except for the Nuku'alofa tide gauge station, which is located at the wharf. These stations provide wind speed (knots), direction, and pressure (hPa) readings

every 10 min. Winds were converted and averaged into hourly winds (m/s) for ease of comparison with modelled winds.

2.3. TC Track Data

TC Harold's best track data from the Australia Bureau of Meteorology (BOM) available at the International Best Track Archive for Climate Stewardship (IBTrACS; [60]) dataset from 12h00 UTC 3 April 2020 to 12h00 UTC 9 April 2020 were used in this study. The dataset has track data available every 3 and 6 h intervals, giving eye location, central pressures, winds, and radius of maximum winds (RMW) at each of the quadrants. Here, we used 6 h intervals only. This study also analysed the best-track data from the dataset of the Joint Typhoon Warning Centre (JTWC) of the US Naval Pacific Meteorology Oceanography Center in Hawaii. The JTWC's radius of maximum winds was three times smaller, its forward speed slower, and its track was moving away from Tonga compared to the BOM track at times when Harold was approaching Tonga (see 36–42 h in Figure 1b). The widely used Southwest Pacific Enhanced Archived of Tropical Cyclones (SPEArTC; [61]) dataset for TC studies in the Southwest Pacific does not archive the radius of maximum winds, a parameter that is important for inducing storm surges and waves, hence the best track data from the SPEArTC dataset is not analysed here. Since there were discrepancies between the different TC track products (e.g., the radius of maximum winds and intensity, the forward speed, direction, and distance of the eye to Tonga), we decided to use the BOM track for this study as it gives the worst-case scenario, i.e., closer, faster, and higher radius of maximum winds than when TC Harold approached Tongatapu.

2.4. Atmospheric Forcing—Dynamic Holland Model

The advantage of using a parametric wind model for modelling waves in a real-time early warning system is that it is simple, fast, and computationally efficient. Consequently, we used the Holland model [41] to provide the atmospheric forcings for the study; however, this published model was based on the parameterisation of a snapshot of instantaneous winds at the gradient wind level, rather than the surface level winds of a developed and dynamically moving TC. Fleming et al. [30] modified the Holland model to dynamically account for a moving and developing TC and implemented it in ADCIRC, which is now commonly referred to as the dynamic Holland model (DHM).

The TC best track data provide the time, position (in latitude and longitude) of the eye of the cyclone, maximum observed wind speed at 10 m (S_f), the radius of maximum wind (R_w), and the central pressure (P_c). At each node of the mesh, wind velocity is computed by the dynamic Holland model using the following steps:

Firstly, the maximum storm wind speed at 10 m (S_m) is calculated by subtracting the storm translation speed from the maximum hindcast or forecast wind speed S_f,

$$S_m = S_f - \sqrt{v_x^2 + v_y^2}$$

where v_x *and* v_y are the forward velocities of the cyclone in the east and the north directions, respectively, obtained from the best track data. The S_m at 10 m obtained is converted to the maximum velocity at the top of the atmospheric boundary layer by multiplying it with the inversion of the boundary layer adjustment factor $\beta = 0.9$,

$$V_m = S_m/\beta$$

where V_m is the gradient wind speed at the radius of maximum winds, R_w

The Holland B parameter is then computed next using the following equation:

$$B = \frac{\rho e V_m^2}{(P_n - P_c)}$$

where ρ is the air density (assumed constant at 1.15 kg·m^{-3}), P_n is the ambient atmospheric pressure, P_c is the storm's central pressure, and e is the Euler's number (e = 2.7182). Based on analysis by Holland [41], if the resulting value of the Holland B parameter is greater than 2.5 or less than 1.0, then the parameter value is limited to these extremes.

The pressure field at a grid defined in polar coordinates (distance of each grid point and angle with respect to the storm centres) is defined by the expression:

$$P(r) = \frac{(P_n - P_c)exp\left(-\left(\frac{R_w}{r}\right)^B\right) + P_c}{\rho_w g}$$

where r is the distance from the node to the centre of the storm, ρ_w is the water density $(1027\ \text{kg}\cdot\text{m}^{-3})$, and g is the gravitational constant. The gradient wind velocity, V_g, is then obtained by substituting the pressure formula into the gradient wind balance equation (i.e., pressure gradient force = Coriolis force + centripetal force):

$$V_g(r) = \sqrt{\left(\frac{R_w}{r}\right)^B - exp\left[1 - \left(\frac{R_w}{r}\right)^B\right]V_m^2 + \frac{r^2 f^2}{4}} - \frac{rf}{2}$$

where f is the Coriolis's parameter, $f = 2\Omega sin\varphi$, with Ω being the earth's rotation velocity (7.2921×10^{-5}rad·s^{-1}) and φ being the latitude.

The raw gradient wind speed is used to calculate a "tapered" version of the storm translation speed that will be added back to the final wind speed at the surface. Because the parametric wind field tapers down as the radius increases, the whole translation speed cannot be supplied to the entire wind field as it would allow the translation speed to overwhelmingly dominate the wind field at a sufficiently high radius,

$$v_{tx}(r) = \left|\frac{V_g(r)}{V_m}\right| v_x$$

$$v_{ty}(r) = \left|\frac{V_g(r)}{V_m}\right| v_y$$

where v_{tx} and v_{ty} are the translational adjustments to the final wind speed in the north and east directions.

The wind velocity field is separated into north and east components at the node location i and multiplied by the boundary layer adjustment factor β to convert the wind velocity at the top of the atmospheric boundary layer to wind velocity at 10 m.

$$V_{ix} = -V_g(r)\beta sin\theta_i$$

$$V_{iy} = V_g(r)\beta cos\theta_i$$

where θ_i is the angle between node i and the centre of the storm.

In the last step, we multiply by the sampling time adjustment (ct = 0.88) to convert 1 min winds to 10 min winds then add the tapered translation velocity to obtain:

$$V_{fix} = c_t V_{ix} + v_{tx}$$

$$V_{fiy} = c_t V_{iy} + v_{ty}$$

where V_{fix} *and* V_{fiy} are the final velocities in the east and north directions, respectively, at node i.

2.5. Model Setup

2.5.1. ADCIRC and SWAN Model Domain

The OceanMesh2D Matlab toolbox [62] was used to produce a triangular unstructured mesh for the area of study (Figure 2a). A mesh of 74,207 nodes with 38,767 triangles was used for the whole domain with a mesh resolution ranging from 50 m nearshore to 1000 m offshore (Figure 2b). The land above the mean high water springs (MHWS) was not included in the mesh and observed stations inland are represented by the closest nodes on the coastline. The study domain includes all the main islands of Tonga.

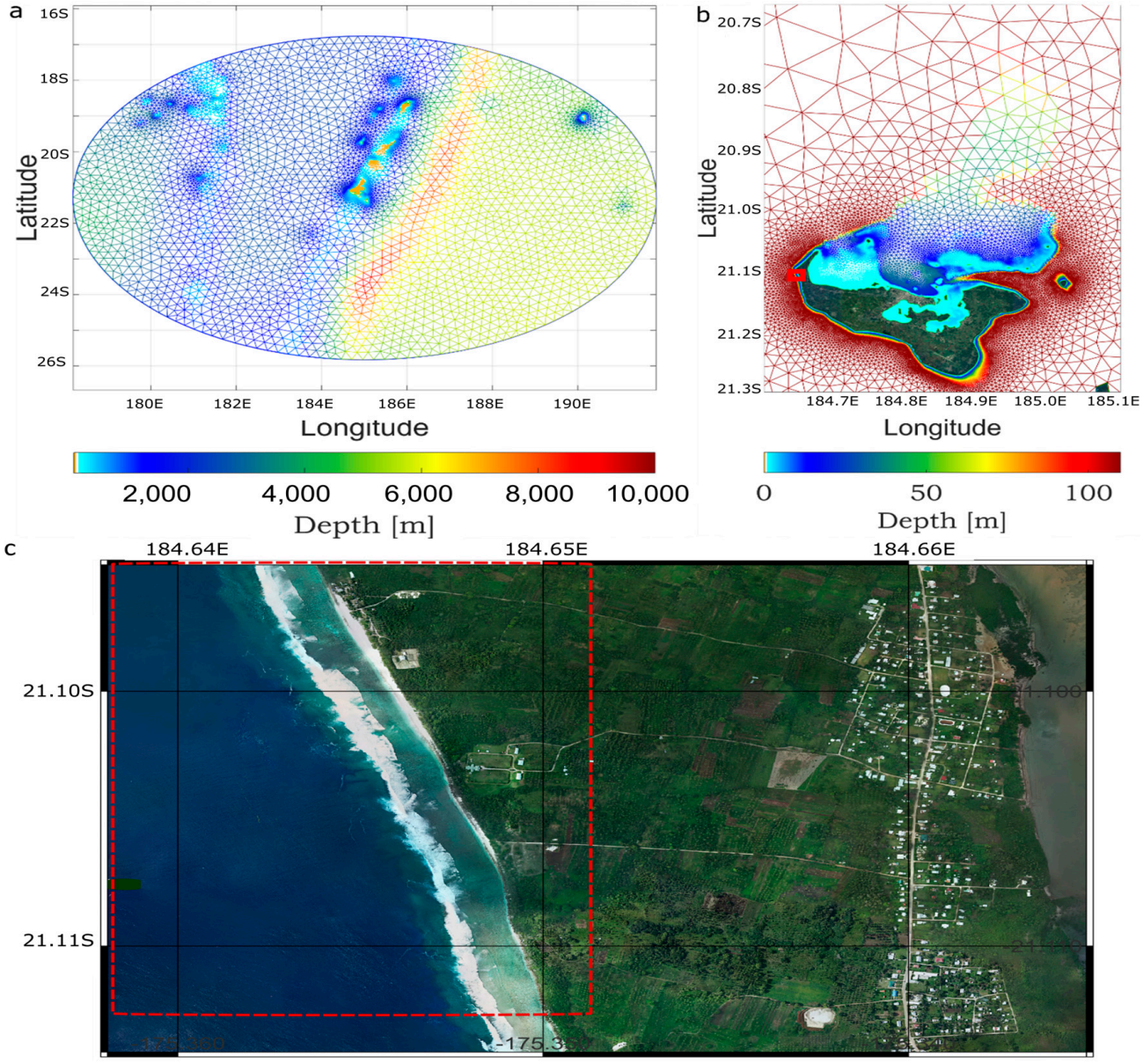

Figure 2. (**a**) Triangular unstructured mesh for Tonga. (**b**) Zoomed-in view of Tongatapu with depths capped at 250 m for a better representation of the shallow shelf and reef system. The red box on the western side is zoomed and shown in (**c**), showing the study site for the XBEACH model.

The 30 m resolution global bathymetry and topography grid (SRTM15+; [63]) database was used to prescribe the bathymetry and topography data over the study domain while applying a local mesh refinement over Tongatapu to leverage the available LiDAR and high-resolution bathymetric data to increase the coastal resolution in Tongatapu (Figure 2b).

The topographic and bathymetric LiDAR data for Tongatapu were obtained from the Pacific Community (SPC), with permission from the Tonga Meteorological Service.

Tongatapu contains extensive tidal flats, coastal marshes, and mangrove forests along the northern boundary to the west of Nuku'alofa. The rest of the shorelines are surrounded by narrow fringing reefs. Along the northern side is a shallow shelf to the west extending northward, inside the inner lagoon and northeast of the island (in cyan colour in Figure 2b). Inside, the lagoon is fringed by mostly mangroves [48]. Tonga has steep-sloped shelves surrounded by deep waters except on the northern side (Figure 2a,b).

2.5.2. ADCIRC and SWAN Models

In the present study, ADCIRC (v55) was coupled with the SWAN (v41.20) wave model (see [31]). The ADCIRC model solves the shallow water equations by computing water levels and currents via solutions of the generalized wave continuity equation and the vertically integrated momentum equations, respectively, with a wetting–drying algorithm all in an unstructured mesh. ADCIRC passes wind fields, water levels, currents, and bottom friction to SWAN. SWAN, in turn, computes the wind waves, radiation stress, and their gradients in the same unstructured mesh. The radiation gradient stress is then passed to ADCIRC to provide additional forcing nearshore for wave setup and currents.

SWAN was run in non-stationary mode with 36 directional and 36 frequency bins. SWAN was forced by the wind velocities, water levels, and currents provided by ADCIRC every 30 min and vice versa. The wave physics package ST6 was used as several studies have shown its benefits, whether it was standalone modelling (e.g., [64]) or coupled modelling. We used the default U10PROXY with windscale = 20 instead of the windscale = 28, which significantly overestimates wave heights. The default Komen formulation as modified by Rogers et al. [65] was used for whitecapping. According to Nelson [66], the breaking parameter for wave breaking caused by changes in depth can be determined by considering the bottom slope and depth, and a value of 0.46 improves the wave setup estimations instead of the default value of 0.54. The bottom friction applied was the Madsen et al. [67] formulation with an equivalent roughness length scale of 0.05 providing a more reasonable wave height than the default bottom friction JONSWAP [68]. The bottom drag formulation was computed using Manning's value of n = 0.22 for reefs [25], and wind drag was computed using the Garratt formulation [69].

The use of unstructured triangular meshes allows for very fine resolution near the coast and much coarser resolution in open waters [31]. Such flexibility allows a realistic representation of where waves and circulation are generated in deep water, propagated, and transformed near the coastline, and hence a better estimation of the storm surge and waves nearshore. ADCIRC + SWAN has been successfully validated against measurements from wave buoys and tide gauges during several past historical tropical cyclones [31,33].

The mesh was configured with an ocean open boundary that was forced with the amplitude and phase of the 8 major tidal constituents for Tonga (i.e., M2, S2, N2, K2, K1, O1, P1, Q1; [59]), which were obtained from the TPX09 database (https://www.tpxo.net/global/tpxo9-atlas; accessed 21 January 2022), to characterise tide variability and validate the model.

2.5.3. XBEACH

The XBEACH model has been widely used to validate the contributions of wave setup and infragravity waves to extreme water levels and coastal inundations on coral reef-lined islands and to enhance understanding of the swell-driven hazards in fringing reef environments (e.g., [53,70,71]). It is a coupled phase-resolving wave and circulation model that resolves the complete wave transformation processes, including swash hydrodynamics.

The XBEACH model was implemented in this study in non-hydrostatic (NH) mode [56] using a 2D approach. In NH mode, dispersive waves are simulated using a depth-average flow model. In a first assessment, the model was set up with the default parameters. At the open boundary, the model was forced with parametric wave conditions (H_s, T_p, θ_p)

and offshore water levels from the coupled ADCIRC + SWAN simulation. The model was applied to a particular coastal segment where the extreme waves from TC Harold provoked structural damage to buildings along the western coast of Tongatapu (Figure 2c). The model was used to examine the contribution of IG waves ($H_{s,IG}$) with frequencies between $f_{min} = 0.0036$ Hz and $f_{max} = 0.033$ Hz (wave periods between 30 s and ~5 min), waves in the sea-swell frequency bands ($H_{s,SS}$) with frequencies between $f_{min} = 0.033$ Hz and $f_{max} = 0.6$ Hz (wave periods between 1.67 and 30 s), and wave setup to the extreme total water level and coastal inundation. Significant wave heights of short $\left(H_{s,SW}\right)$ and IG waves ($H_{s,IG}$) were calculated from the partially integrated power spectrum:

$$H_s = 4\sqrt{\int_{f_{min}}^{f_{max}} E(f)df}$$

2.6. Experiment Design

In the present study, we carried out 7 modelling experiments (see Table 1) including running ADCIRC as a standalone model and ADCIRC coupled with SWAN to simulate the total water level (TWL) and storm surge with respect to the tide, wind surge, inverted barometer effect, and wave-driven surge. All simulations were initialized in cold start mode for a 3 day model spin-up. The model results between 12h00 UTC 6 April 2022 and 12h00 UTC 9 April 2020 were compared with the observed data at the Nuku'alofa station.

Table 1. Descriptions of the set of experiments conducted.

Experiment (Exp.)	Model Description
1	ADCIRC + SWAN (astronomical tide and atmospheric forcings)
2	ADCIRC standalone (astronomical tide and atmospheric forcings)
3	ADCIR + SWAN (atmospheric forcing plus wave gradient forcing)
4	ADCIRC standalone (atmospheric forcing only)
5	ADCIRC standalone (air pressure only)
6	ADCIRC standalone (astronomical tide forcing only)
7	XBEACH to test the influence of waves on the inundation

Following Joyce et al. [27], the contributions of each forcing is determined by analysing the differences between successive experiments. In particular, we compared the performance of coupled versus uncoupled model runs first, then we evaluated the relative contributions of each of the forcings to the total water levels and storm surges by removing one of the forcings. In experiments (Exp.) 1 and 2, we evaluated the total water levels of coupled (ADCIRC + SWAN) versus uncoupled (ADCIRC only) simulations forced with the tide, pressures, and winds. The difference between Exp. 1 and 3 was used to evaluate the contributions of the tide; 3 and 4, the wave setup; and 4 and 5, wind surge. Exp. 5 gives the contribution of the atmospheric pressures. Exp. 6 compared the simulated tide (ADCIRC standalone forced only with astronomical tides) against predicted tides from COSPPac. In the final experiment (Exp. 7), we forced the XBEACH model with outputs from the coupled ADCIRC and SWAN simulations to obtain the contribution of wave setup and infragravity waves to the total water levels and runup. Figure 3 shows a flowchart simplifying modelling steps.

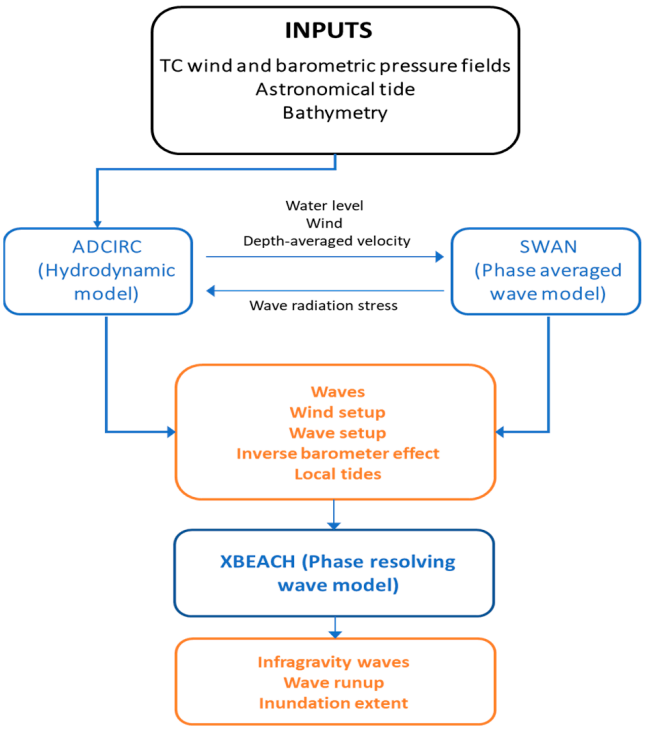

Figure 3. A simplified flowchart of the model steps. The initial input is shown in the black box at the top of the flowchart, the models are shown in blue boxes, and model outputs are shown in orange boxes. The blue arrows indicate the flow of information.

3. Results and Discussions

3.1. Validating the Dynamic Holland Model Performance

We applied the DHM wind parametric model to the BOM best track TC Harold data to obtain the pressure and wind fields required for the storm surge and wave simulation. The best track data were reformatted and read directly into ADCIRC by the DHM parametric wind model to compute the wind stress and barometric pressures. Surface model winds and pressures were compared against observations from the six stations of the observation network of the TMS (Figures 4 and 5, respectively). The barometric pressures and winds simulated by the DHM have their peaks comparable in both magnitude and phase with the observations in all of the AWS and the tide gauge station. An overall root mean square error (RMSE) of 3.03 hPa and 2.84 m/s for the model barometric pressures and winds, respectively, against observations are shown in Table 2 (see rows 1 and 2).

3.2. Astronomical Tide

We used the eight major tidal constituents from the TPXO global tide model to force ADCIRC (v55) at the open boundaries. ADCIRC reproduces the tidal phase and amplitude accurately compared to the Nuku'alofa tide gauge station (Figure 6a); however, the ADCIRC model slightly overestimated the low tides (overall RMSE of 0.3 cm; see row 3 in Table 2). Further experiments, for example, with longer time spans of up to two to three weeks would be needed to produce better predictions of the astronomical tides in Nuku'alofa.

3.3. Total Water Level (TWL) and Storm Surge Validation

The coupled ADCIRC + SWAN model was run in standalone mode forcing with the astronomical tide and atmospheric forcings, as well as the wave radiation stress, whereas the uncoupled ADCIRC model was only forced by the astronomical tide and atmospheric forcings. Overall, the coupled simulation results in a higher total water level (TWL) particularly on the reefs surrounding the islands as the simulation includes the effect of wave setup (Figure 7a). Consequently, the storm surge at the location of the tide gauge

station is better resolved (peak storm tide of about 1.5 m; Figure 7a) than in the uncoupled simulations (about 1.25 m; Figure 7b)—a difference of 0.25 m accounting for 20% more water with the coupled run. The RMSEs for the coupled and uncoupled TWLs were 6.7 cm and 8.9 cm, respectively (see rows 4 and 5 in Table 2).

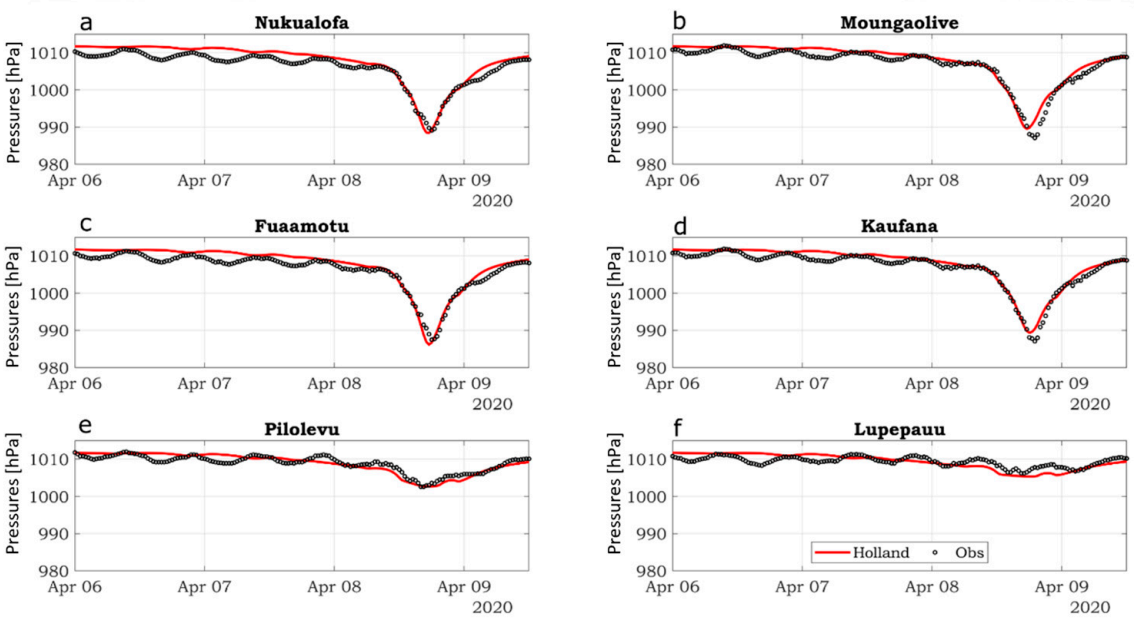

Figure 4. Comparison of the barometric pressure (hPa) evolution obtained from feeding the DHM with the BOM best track TC Harold data (red) versus observations (black) at the (**a**) Nuku'alofa tide gauge, and the AWSs located at (**b**) Mounga'olive (**c**) Fua'amotu airport, (**d**) Kaufana airport, (**e**) Pilolevu airport, and (**f**) Lupepau'u airport from 6 April 12h00 UTC to 9 April 12h00 UTC.

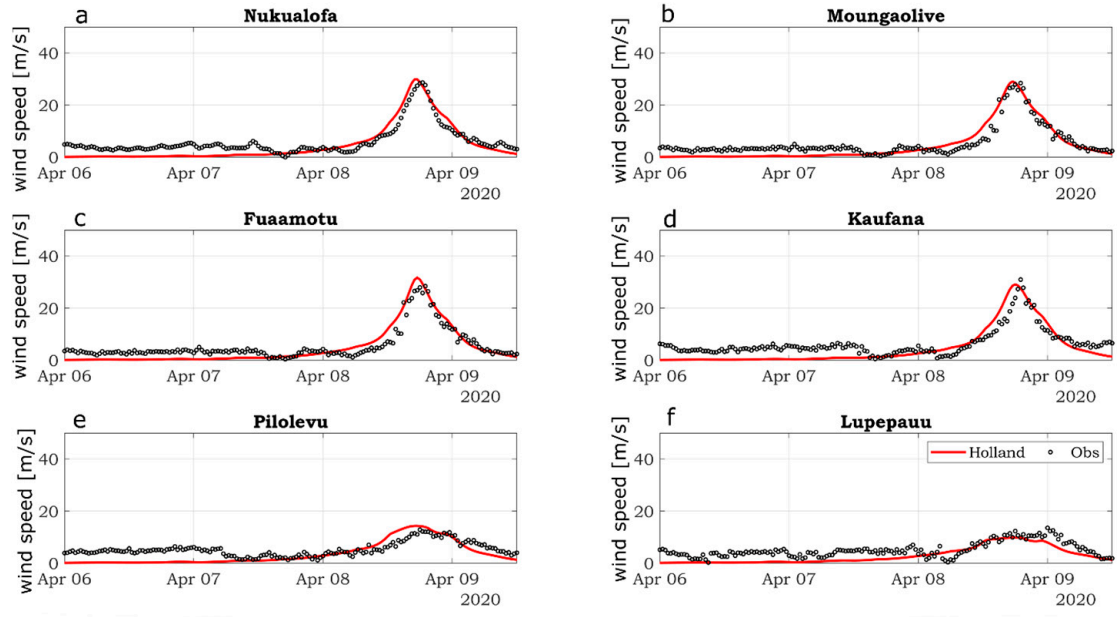

Figure 5. Comparison of the wind speed (m/s) obtained from feeding the DHM with the BOM best track TC Harold data (red) versus observations (black) at the (**a**) Nuku'alofa tide gauge, and the AWSs located at (**b**) Mounga'olive, (**c**) Fua'amotu airport, (**d**) Kaufana airport, (**e**) Pilolevu airport, and (**f**) Lupepau'u airport from 6 April 12h00 UTC to 9 April 12h00 UTC.

Table 2. Root mean square errors (RMSEs) for the models' performance.

	Model vs. Observations	RMSE
1	Model pressures—Figure 4	3.03 hPa (overall)
2	Model winds—Figure 5	2.84 m/s (overall)
3	Tide (COSPPac vs. ADCIRC)—Figure 6a	0.30 cm
4	Coupled model TWL (Exp. 1)—Figure 6b	6.7 cm
5	Uncoupled model TWL (Exp. 2)—Figure 6b	8.9 cm
6	Model storm surge coupled run with no tide (Exp. 3)—Figure 6c	3.5 cm
7	Model storm surge (Exp. 2–Exp. 6)—Figure 6c	7.8 cm
8	Model storm surge (Exp. 1–Exp. 6)—Figure 6c	4.6 cm
9	Linearly adding tide to the storm surge run without tide (Exp. 6 + Exp. 3)—Figure 6b	7.03 cm (overall)

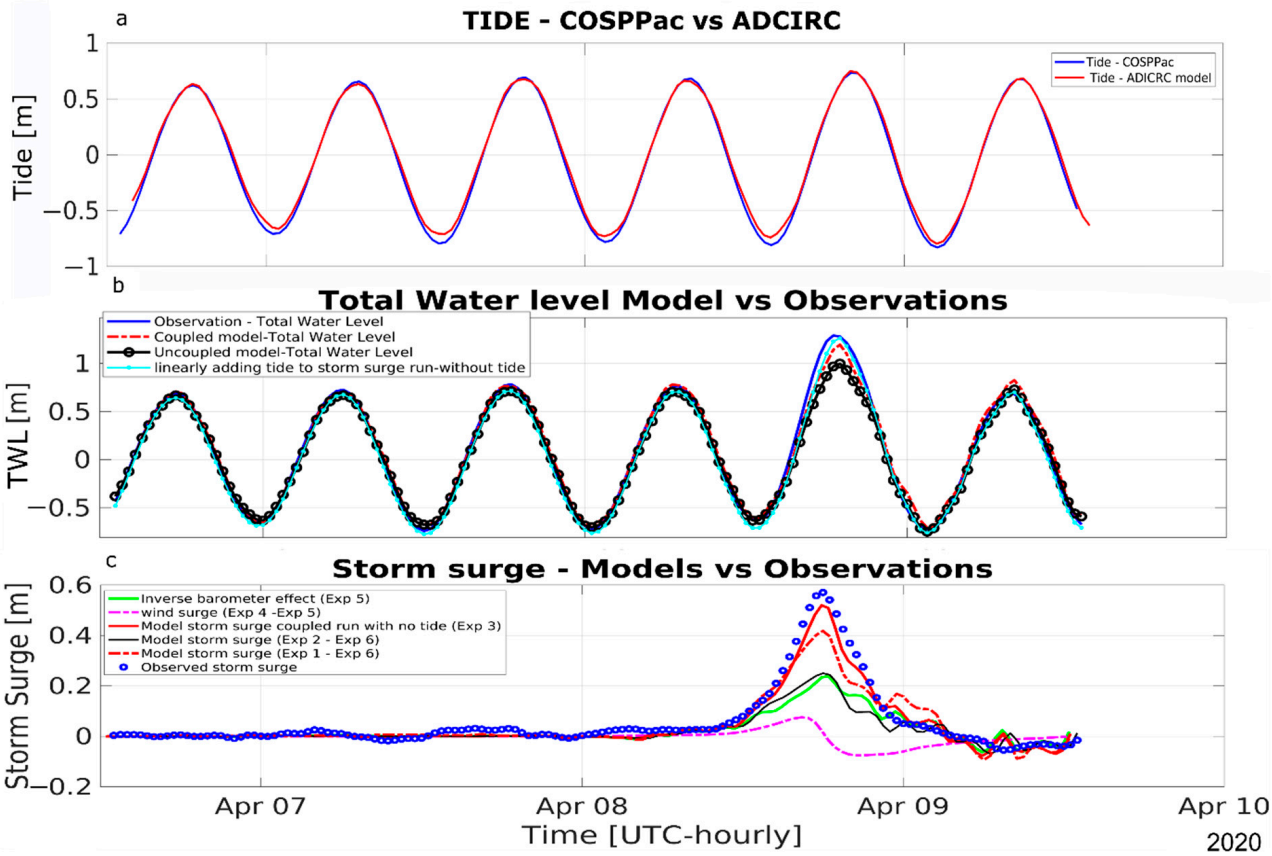

Figure 6. (**a**) ADCIRC predicted tide (in red) versus the COSPPac tide (in blue) at the Nuku'alofa tide gauge station from 12h00 UTC, 6 April 2020 to 12h00 UTC, 9 April 2020, with a cold state-run of 3 days (not shown). (**b**) Comparison of observed (in blue) and modelled total water levels (coupled (in red), uncoupled (in black), and linearly adding tide with storm surge run without tide (in cyan)). (**c**) A close-up view of the peak storm surge recorded at the Nuku'alofa tide gauge station (in blue) as well as the relative contributions of the model wind (in magenta), inverted barometer effects (in green), total model storm surge (coupled without tide—in red), total model storm surge (uncoupled without tide—in black), and model storm surge (in red dashed line).

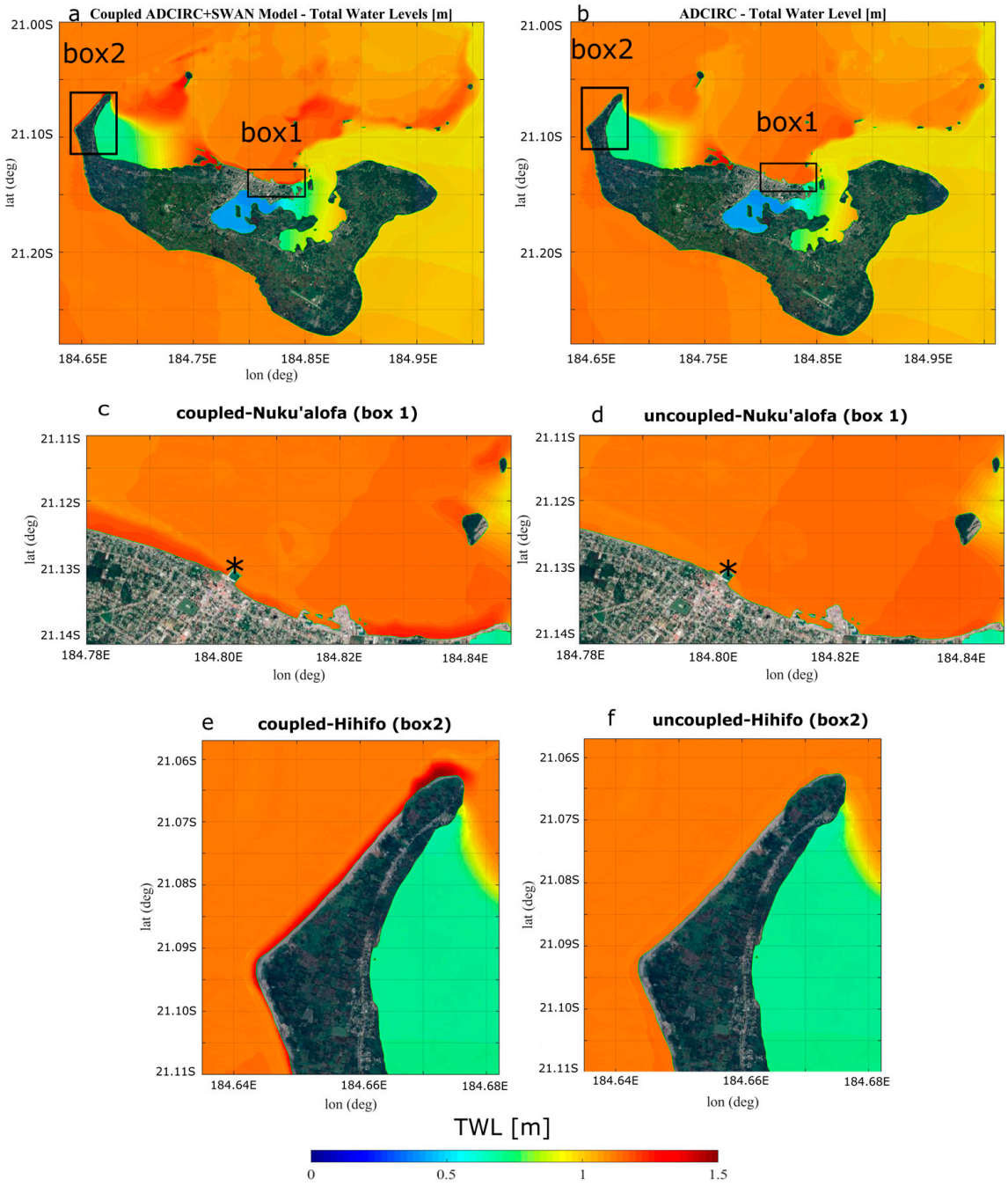

Figure 7. Spatial maps of maximum storm surge levels (in meters) for Tongatapu from (**a**) coupled and (**b**) uncoupled runs. The black boxes are Hihifo (left—box 2) and Nuku'alofa (right—box 1) and are enlarged, respectively, in (**c**,**e**) (coupled run vs. uncoupled—Nuku'alofa) and (**e**,**f**) (coupled run vs. uncoupled—Hihifo). The black asterisks in (**c**,**d**) are the locations of the tide gauge.

In addition, Figure 6b shows a comparison of the time series of the computed TWL from the coupled and uncoupled runs at the closest node to the tide station in Nuku'alofa against observations. The simulated TWL peaked around the same time as the observed at ~18h00 UTC, 8 April 2020 with a height of ~1.19 m, ~9 cm less than the observed TWL or 19 cm more than the TWL obtained from the uncoupled run. The underestimation of the observations by the coupled model peak by 9 cm may be mainly due to the model resolution not being high enough to better resolve wave-breaking processes on the reefs near the tide gauge station and/or the lack of land cover information and corresponding

Mannings friction coefficients to better resolve peak, current, and wave interaction on the reef flat [32].

3.4. Relative Contributions of Different Forcings to the Total Water Levels

The computed total water level is a combination of the relative contributions of the tide, wave setup, wind effect, and pressure; however, these components are affected in different ways by various factors, such as the location of the island relative to the moving TC, the bathymetry and topography, the intensity and the direction of the winds, and the timing of the tide.

3.4.1. Wave Setup

The computed maximum significant wave heights offshore were up to 12 m (Figure 8a). Despite having no in situ data to validate, this maximum significant wave height is reasonable compared with the satellite altimetry from the NOAA/STAR Laboratory for Satellite Altimetry (LSA) which captured large waves up to 9.3 m between 07 00h00 and 12h00 UTC when TC Harold was approaching Fiji from the west, and up to 12.5 m between 09 12h00 and 23h59 UTC when TC Harold was 1200 km to the southeast of Nuku'alofa.

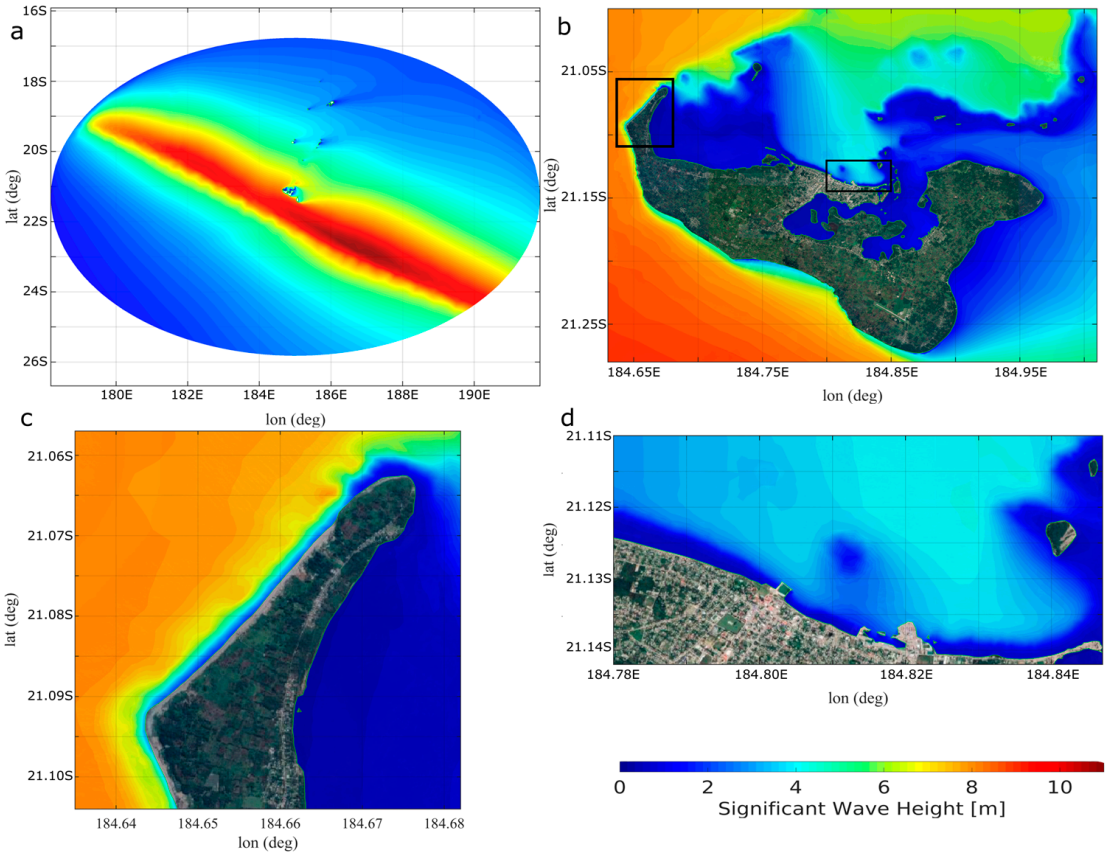

Figure 8. Significant wave heights over the (**a**) study area, and a zoomed-in view over (**b**) Tongatapu, (**c**) Hihifo (left box in **b**) and (**d**) Nuku'alofa (right box in **b**).

Unlike broad mild slope continental shelves that attenuate wave heights before they approach the nearshore, Tongatapu is no different to other Pacific island countries, with very narrow shelves and steep bathymetry where wave breaking in such proximity gives rise to large coastal total water level effects nearshore. This is the case on the western side of the island, Hihifo, facing large waves as high as 5–6 m breaking on the reefs (see Figure 8a–c), where wave setup was more prominent (see Figure 9a–e) with up to ~1.1 m, accounting for more than 75% of the total water levels in this area. In contrast, reefs in the north-facing Nuku'alofa experienced smaller waves of about ~2.5–3 m, resulting in a wave

setup of ~0.3 m on the reef flats or ~20% of the total water levels (see Figure 9a–e). This simulated wave height is consistent with the large and severe waves that occurred less than 1% of the time in a year and more than 3.0 m in Nuku'alofa [10].

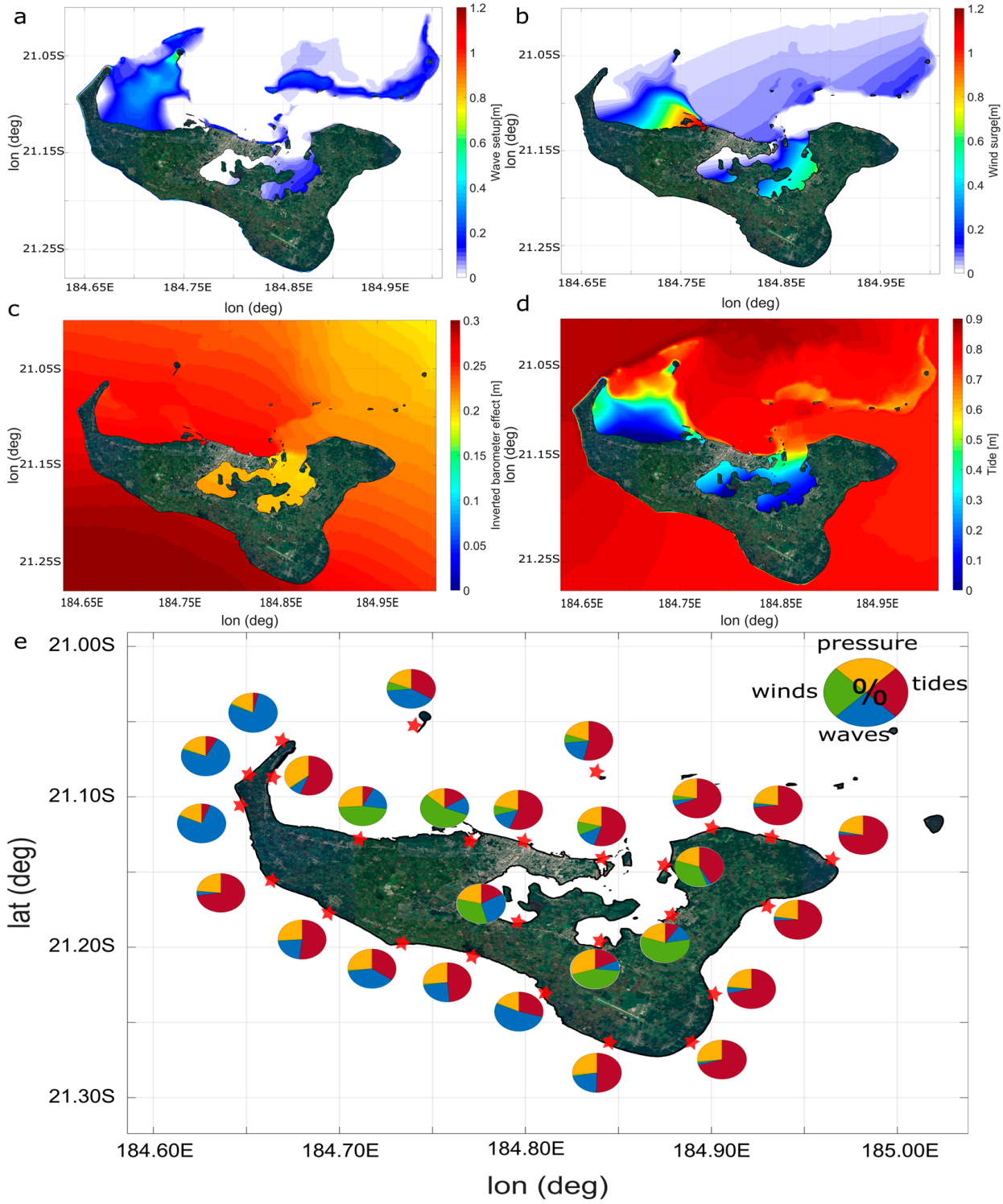

Figure 9. Spatial maps representing the relative contributions of (**a**) wave setup, (**b**) wind surge, (**c**) inverted barometer effect, and (**d**) tide to the total water levels (m) in Tongatapu. (**e**) Pie charts represent the relative contributions of wave setup, wind surge, inverted barometer effect, and tide to the total water levels (m) in selected points (red stars) near villages along the shoreline around Tongatapu.

3.4.2. Wind Setup

TC Harold's spatial wind and pressure fields were computed using the DHM parametric wind model based on the BOM best track data. Figure 9b shows the maximum wind surge contribution to the overall TWL. As TC Harold tracked southeastward to the west and southwest of Tonga, the strong northwest winds equatorward, which reached up to 30 m/s, as observed in the Nuku'alofa tide gauge station (Figure 4), resulted in maximum wind surges that could be seen in the coastal area immediately to the west of Nuku'alofa (more than 50% of TWL) and two coastal stretches inside the lagoon (30–40% of TWL). These areas could be characterised by shallow shelves (in cyan colour in Figure 2b) and narrow concave coastlines with relatively uniform water depth facing the strong northwest winds, which may have largely contributed to the maximum wind surge. On the contrary, on the western side, Hihifo, which was facing the winds, the wind surge effect was small and similar to the southern and eastern sides, which were sheltered from or lying parallel to the strong northwest winds. This can be explained by the steeply sloped bathymetry with narrow fringing reefs in these areas. As can also be seen along the coastline of Nuku'alofa (see Figure 9b), wind surges from the west and northwest pile up in the east, indicating the bathymetry in Nuku'alofa is rising gradually from west to east, making this part of Nuku'alofa a more favourable area for wind surges for TCs approaching Tongatapu from the northwest.

3.4.3. Atmospheric Pressures

Figure 9c shows the inverted barometer effect over Tongatapu, with a contribution to the coastal total water level ranging from ~0.20 m on the northeastern side to ~0.30 m on the southwestern side, except inside the lagoon, where the contribution was a little lower. This may be due to shallower body of water in the lagoon compared to larger body of water in the deep open ocean for the atmospheric pressure to have an effect. In general, relative to its contribution to the total water level around Tongatapu, the inverted barometer effect contributions seem relatively uniform in magnitude (~25% of TWL) compared to other components (see Figure 9e), which varied extensively.

3.4.4. Tides

Figure 9d shows ~10 cm higher offshore tide levels in the west of Tongatapu at the time of TC Harold's landfall; however the tidal contribution to the TWL nearshore was minimal in the west compared to the east (Figure 9e; 5–10% vs 50–75%). This can be explained by the large wave setup contribution that dominates TWL along the west facing shoreline due to the direct impact of large waves from the west. Similarly, areas with shallow shelves such as those immediately to the west of Nuku'alofa and inside the lagoon also showed minimal tide contribution (5–10%) as wind setup was the predominant contributor in these areas. In contrast, in areas that were sheltered from or lying parallel to the strong northwest winds and large waves, such as the eastern and southern sides of the island, the tide was dominant (more than 50%; Figure 9e).

The findings of this study are similar to those found in other regions with steeply sloped shelves around the world. For example, Joyce et al. [27] examined the waves and storm surge for 2017 TC Irma and Maria and found that wind surge was dominant in shallow shelves and wave setup in steeply sloped regions in Puerto Rico and the U.S. Virgin Islands; however, the barometric pressure was generally the dominant contributor to the extreme water levels, perhaps simply because the eyes of these TCs moved across these islands. In contrast, TC Harold's eye's closest distance was 110 km to the south of Tongatapu, so the effects of the atmospheric pressures were not that large, though they appeared uniform. Additionally, several studies have also found that lower/higher wave setup occurred in areas with a mild/steep slope (e.g., [25–27,34,72]).

3.5. Storm Surge—With and without Tides

We can obtain storm surge from simulations by either including or not including tidal forcing. Without tidal forcing (i.e., forced by atmospheric forcing only), the computed storm surge was comparable to the observed storm surge (53 cm (red) vs. 58 cm (blue), respectively, in Figure 6c; RMSE = 3.5 cm-see row 6 in Table 2); however, when the astronomical tide forcing was included, the storm surge was ~42 cm (RMSE = 7.8 cm-see row 7 in Table 2) or ~11 cm lower than the storm surge computed without tide. Particularly, without the influence of the tide, the wave setup could reach a maximum height of ~25 cm and decrease to ~15 cm when the tide is included. This indicates the nonlinearities of tide and storm surge interaction, which results in lower/higher wave setup during high/low tide.

Since Tongatapu lies in a shallow, broad region that is influenced by strong currents with eddies due to the abrupt changes in the depth between the eastern and western sides [57], it is possible that these strong currents can enhance the nonlinear interaction between the tide and storm surge, resulting in weakening the energy of the storm surge as it approaches Tongatapu, especially on the northern shoreline.

Additionally, this may be due to fewer waves breaking on the reefs and the stronger undertow during high tide, resulting in a lower wave setup during high tide. In contrast, when the TC occurs during low tide, more waves break onto the reef crest, and the undertow is weaker, allowing the wave setup to increase. In addition, the uncoupled storm surge (black coloured line in Figure 6c) was ~0.23 cm, or 30 cm lower than the coupled storm surge without the tide (or 19 cm lower than the coupled storm surge minus the tide). The RMSE was 4.6 cm (see row 8 in Table 2).

Figure 6b also shows the TWL obtained from the linear addition of the tide with the coupled storm surge run without tide (cyan) with its peak closely matching the observed peak in the tide gauge station (~3 cm less); however, overall RMSE = 7.01 cm (see row 9 in Table 2). These results may imply the prospect, especially in the operational environment, and the need to develop a fast, and light coastal inundation warning system for Tonga. Ideally, the fully coupled model is run to resolve all necessary physics. However, linearly adding tides to the model output yields similar results especially in the peak TWL. To account for uncertainties of landfall in such a forecast system one option is to run the coupled model and then manually add the tidal signals with different temporal offsets. Doing so would provide a range of possible future scenarios or uncertainties, where risk thresholds can be developed based on a specific criteria. While this method would allow a fast assessment, it might introduce errors in shallow areas where wind and wave setup dominate.

3.6. Total Water Level and Coastal Inundation

The XBEACH model was run in 2D non-hydrostatic mode to evaluate the contribution of wave setup and infragravity waves as the primary mechanisms driving inundation in many reef-fronted sections. We applied the XBEACH model at a segment of the coastline at Hihifo, which experienced extreme coastal inundation that led to structural damage, including at the Royal residence Liukava [73]. Since there were no pressure sensors in Tonga to gauge wave setup and infragravity waves during TC Harold, we qualitatively validated the coastal inundation map using Google Earth images taken before (Figure 10a) and after (Figure 10b) TC Harold. It can be seen from the satellite imagery after the event that the inundation debris indicates the extent of the flooding at about 80 to 120 m inland (red dashed line in Figure 10d).

Wave parametric conditions (period = 12.1 s, significant wave height = 7.5 m, and direction = 337.4°) and water levels (0.782 m) at a point ~900 m offshore obtained from the coupled model were used as boundary conditions. The simulation shows (Figure 2c) that the TWL nearshore reconfirms the dominance of the wave setup (solid red line in Figure 10c) with a magnitude comparable to the coupled ADCIRC + SWAN run (green line). Additionally, infragravity waves (red dashed line) and waves in the sea/swell frequency range (dotted red lines) were also dominant.

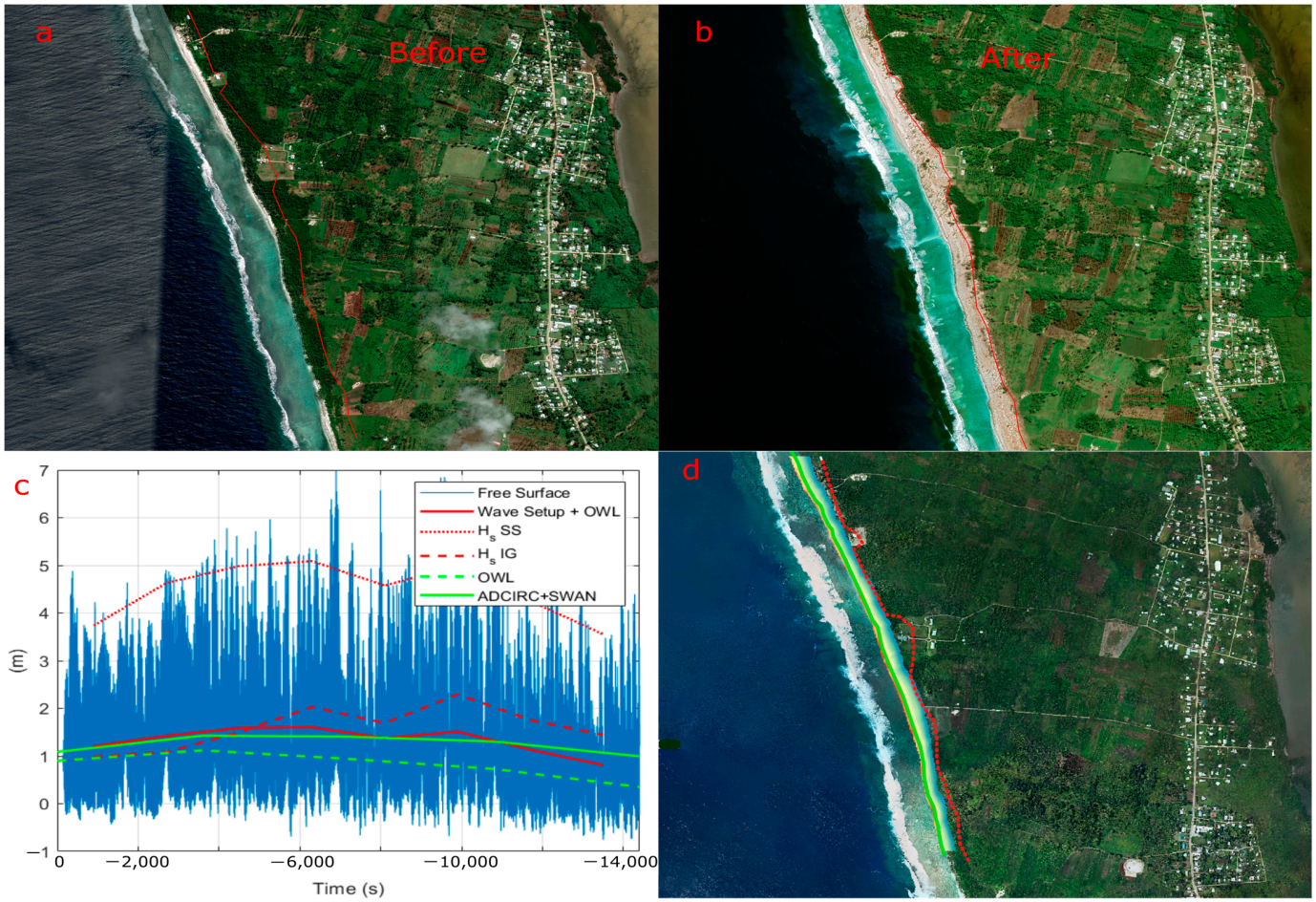

Figure 10. A satellite picture from Google Earth taken (**a**) before (July 2019) and (**b**) after (May 2020) TC Harold; inundation debris is visible from the satellite after the event and the inundation extent is marked with a red line. (**c**) The infragravity waves (red dashed line), wave setup (red line), significant wave height of seas and swells, offshore water level at a point 900 m offshore. (**d**) The extreme total water level from the coupled ADCIRC + SWAN run (green line), wave runup, and the satellite inundation extent (red dotted line).

Figure 10d shows the spatial distribution of the inundation depth and extent from the XBEACH simulations, the inundation extent from the satellite imagery (red dotted line; Figure 10b), and maximum TWL from the coupled ADCIRC + SWAN run (green line). The flood extent from the XBEACH run was comparable with the satellite imagery, especially in areas where natural vegetation is intact. Total water levels from ADCIRC+SWAN underestimated the inundation extent by 80–100 m as infragravity waves are not considered by these models. XBEACH slightly underestimated the runup where the vegetation has been removed for buildings and roads. To account for this, varying bottom and land friction coefficients can be applied to the model domain (e.g., [74]); however, this is beyond the scope of this study.

Results from the XBEACH run indicate that wave setup is not the only contributor to extreme TWL nearshore; infragravity waves also play a major role. Hence, the coupled ADCIRC + SWAN run should be used cautiously, especially in sites where waves dominate. Nonetheless, this result highlights the importance of coupling hydrodynamics, waves, and inundation models for a full coastal inundation forecasting early warning system.

4. Conclusions

In this study, we explore the performance of the coupled ADCIRC + SWAN and the uncoupled ADCIRC standalone simulations in resolving nearshore water levels induced

by tropical cyclone (TC) Harold on 9 April 2020 in Tonga. In particular, we investigate the relative contribution of different forcings (wind surge effect, inverted barometer effect, wave setup, and tide) on the observed water levels along Tongatapu. We applied the dynamic Holland model to the Bureau of Meteorology's (BOM) best track data to obtain the atmospheric forcing represented in the form of winds and barometric pressure fields for the experiments. We also used output from the coupled ADCIRC + SWAN to force the XBEACH model on a coastal segment of Hihifo (the western side of the island), where the inundation was very damaging, to evaluate the contribution of wave setup and infragravity waves. The results can be summarised as follows:

When combining waves and atmospheric forcings (wind and pressure), the coupled ADCIRC + SWAN simulation increases the water level along the reef flats between 20% (in the Nuku'alofa tide gauge) and 75% (in Hihifo) when compared to the uncoupled simulation due to the contribution of the additional radiation stress gradient forcing. This highlights the importance of including waves to predict coastal inundation in reef-fronted coastlines (steep slope shelves with narrow reefs) that characterise Tonga, in particular, and other islands in the Pacific region. This supports the recommendation by Dietrich et al. [34] that in all coastal applications, waves and circulation processes should be combined or coupled.

In terms of storm surge, the coupled model provided results comparable to observations, with a small underestimation when tidal forcing was included. This highlights the nonlinear relationship between the tide and storm surge, plausibly enhanced by the strong current and eddies due to abrupt changes in the depth between the eastern and western sides of Tongatapu, resulting in a lower storm surge; however, further research in this area is needed to better resolve the non-linear interactions between the tide and storm surge, such as sensitivity studies with different wind drag coefficients and higher mesh resolution.

With its narrow fringing reefs and steeply sloped shelves, larger waves from the west breaking on the reefs led to larger radiation gradient stresses and dramatically increased the wave setup, especially on the western side of the island. Almost concurrently, the shallow shelves immediately to the west of Nuku'alofa and inside the lagoon, lying perpendicular to the strong northwest winds, were dominated by the wind setup accounting for more than 50% and 30–40% of total water level (TWL), respectively. Along the wave-sheltered and on the leeward side of the prevailing winds during TC Harold, water levels were dominated by the tide, which accounts for 50–75% of TWL. The atmospheric pressures contributed uniformly (~25% of TWL), indicating their effects depend mainly on the intensity and distance of the eye of the TC to the island. Notably, these results indicate how coastal geomorphology controls nearshore processes and, in turn, modulates the contribution of each component to the TWL at the shore.

Although wind surge is not the dominant contributor as in mild continental shelves, generally these findings indicate that these components (wave setup, wind surge, atmospheric pressure, and tide) should be considered equally as they may have distinct impacts around the coastlines depending on the distance of the eye, angle of approach, and the intensity of the TCs. In addition, the coupled ADCIRC + SWAN model can be used as a storm surge forecast system on reef fronted islands, providing larger and more realistic estimates of TWL compared to the hydrodynamic model alone (e.g., ADCIRC; JMA storm surge model; sea, lake and overland surges from hurricanes (SLOSH) model, and so on).

However, storm surge forecast should not be used as a stand-alone system to predict coastal inundation in the Pacific region especially along reef-fronted shoreline. To adequately account for the effect of waves, the offshore ocean conditions obtained from the coupled model were used as input into XBeach.

While the XBEACH model produced a wave setup similar to ADCIRC + SWAN, it includes the capacity to generate infragravity waves and inundation overland, that phase-averaged wave models fail to resolve; therefore, these results provide an alternative for a TC inundation forecast system and flood forecasting early warning system (EWS) based on ADCIRC, SWAN, and the XBEACH model. Phase-resolving wave models, however, are

computationally expensive and usually hinder their use in operational mode. An alternate approach is to make use of the advanced surrogate models where waves and inundations are precomputed based on high-fidelity, high-resolution models, and a forecasting system can be developed based on this database (e.g., [75–77]). The use of a surrogate model is considered for future studies. For now, a potential light, fast and efficient TC driven coastal inundation forecasting system can be developed, where tide and storm surge are run separately and then linearly added for different temporal offsets or atmospheric forcings. Besides, the predicted wave field can be used to identify coastlines most exposed to wave driven inundation.

Author Contributions: Conceptualization, M.T. and A.E.; methodology, M.T., A.E. and M.W.; software, M.T., A.E. and M.W.; validation, M.T., A.E. and M.W.; formal analysis, M.T., A.E. and M.W.; investigation, A.E.; resources, A.S., H.D. and Z.B.; data curation, A.E.; writing—original draft preparation, M.T.;writing—review and editing, M.T., A.E., M.W., A.S., H.D. and Z.B.; visualization, M.T., A.E. and M.W.; supervision, A.S., H.D. and M.W.; project administration, A.S. and H.D. All authors have read and agreed to the published version of the manuscript.

Funding: This research received no external funding.

Institutional Review Board Statement: Not applicable.

Informed Consent Statement: Not applicable.

Data Availability Statement: All data used in the study are publicly available except for the observed data of the Tonga Meteorological Service archived at NIWA, and the bathymetric data of Tongatapu.

Acknowledgments: We sincerely thank Taylor Gasher for fixing the bug in the ADCIRC source code, enabling wind to spin clockwise in the Southern Hemisphere. We extend our sincere gratitude to the Tonga Meteorological Service for providing the AWS data and their endorsement of using the LiDAR data for Tongatapu. We thank the COSPPac project for providing the tide observations and predictions data for the Nuku'alofa tide station as well as for funding the publication of this research. Finally, we thank you the Pacific Scholarship for Excellence in Research and Innovation (PSERI) from the University of the South Pacific, Fiji for supporting the first author's studies.

Conflicts of Interest: The authors declare no conflict of interest.

Notes

[1] Storm surge is the elevation in sea levels due to the combined effects of inverted barometric pressures and wind stress associated with a passage of a TC.

[2] Storm tide is the water level that results from the combination of the storm surge and the astronomical tide.

References

1. World Bank. Pacific Catastrophe Risk. Assessment and Financing Initiative (PCRAFI) Project. 2007. Available online: https://documents1.worldbank.org/curated/en/251921468291332622/pdf/949860WP0Box38000Country0Note0Tonga.pdf (accessed on 20 April 2022).
2. Terry, J.P. *Tropical Cyclones: Climatology and Impacts in the South Pacific*; Springer Science & Business Media: New York, NY, USA, 2007.
3. Chand, S.S.; Walsh, K.J. Tropical cyclone activity in the Fiji region: Spatial patterns and relationship to large-scale circulation. *J. Clim.* **2009**, *22*, 3877–3893. [CrossRef]
4. Needham, H.F.; Keim, B.D.; Sathiaraj, D. A review of tropical cyclone-generated storm surges: Global data sources, observations, and impacts. *Rev. Geophys.* **2015**, *53*, 545–591. [CrossRef]
5. Quataert, E.; Storlazzi, C.; van Rooijen, A.; Cheriton, O.; van Dongeren, A. The Influence of Coral Reefs and Climate Change on Wave-Driven Flooding of Tropical Coastlines. *Geophys. Res. Lett.* **2015**, *42*, 6407–6415. [CrossRef]
6. Vitousek, S.; Barnard, P.L.; Fletcher, C.H.; Frazer, N.; Erikson, L.; Storlazzi, C.D. Doubling of Coastal Flooding Frequency within Decades due to Sea-Level Rise. *Sci. Rep.* **2017**, *7*, 1399. [CrossRef] [PubMed]
7. Church, J.A.; White, N.J.; Hunter, J.R. Sea-Level Rise at Tropical Pacific and Indian Ocean Islands. *Glob. Planet. Chang.* **2006**, *53*, 155–168. [CrossRef]
8. Nurse, L.A.; McLean, R.F.; Agard, J.; Briguglio, L.P.; Duvat-Magnan, V.; Pelesikoti, N.; Tompkins, E.; Webb, A. Small islands. In *Climate Change 2014: Impacts, Adaptation, and Vulnerability. Part B: Regional Aspects. Contribution of Working Group II to the*

Fifth Assessment Report of the Intergovernmental Panel on Climate Change; Cambridge University Press: Cambridge, UK, 2014; pp. 1613–1654.
9. Nerem, R.S.; Beckley, B.D.; Fasullo, J.T.; Hamlington, B.D.; Masters, D.; Mitchum, G.T. Climate-change–driven accelerated sea-level rise detected in the altimeter era. *Proc. Natl. Acad. Sci. USA* **2018**, *115*, 2022–2025. [CrossRef]
10. Begg, Z.; Damlamian, H. *COSPPac Wave Climate Reports*; Pacific Community (SPC): Nuku'alofa, Tonga, 2022. Available online: https://oceanportal.spc.int/portal/library/ (accessed on 20 April 2022).
11. WMO. *State of the Climate in the South-West Pacific 2021*; WMO-No. 1302; World Meteorological Organization: Geneva, Switzerland, 2022.
12. von Schuckmann, K.; Le Traon, P.Y.; Smith, N.; Pascual, A.; Djavidnia, S.; Gattuso, J.P.; Grégoire, M.; Aaboe, S.; Alari, V.; Alexander, B.E.; et al. Copernicus marine service ocean state report, issue 5. *J. Oper. Oceanogr.* **2021**, *14* (Suppl. 1), 1–185. [CrossRef]
13. Kuleshov, Y.; Qi, L.; Fawcett, R.; Jones, D. On tropical cyclone activity in the Southern Hemisphere: Trends and the ENSO connection. *Geophys. Res. Lett.* **2008**, *35*, 1–5. [CrossRef]
14. Murakami, H.; Delworth, T.L.; Cooke, W.F.; Zhao, M.; Xiang, B.; Hsu, P.C. Detected climatic change in global distribution of tropical cyclones. *Proc. Natl. Acad. Sci. USA* **2020**, *117*, 10706–10714. [CrossRef]
15. Knutson, T.R.; Chung, M.V.; Vecchi, G.; Sun, J.; Hsieh, T.L.; Smith, A.J. Climate change is probably increasing the intensity of tropical cyclones. *Crit. Issues Clim. Chang. Sci. Sci. Brief Rev.* **2021**. [CrossRef]
16. Andrew, N.L.; Bright, P.; de la Rua, L.; Teoh, S.J.; Vickers, M. Coastal proximity of populations in 22 Pacific Island Countries and Territories. *PLoS ONE* **2019**, *14*, e0223249. [CrossRef] [PubMed]
17. Kumar, L.; Taylor, S. Exposure of coastal built assets in the South Pacific to climate risks. *Nat. Clim. Change* **2015**, *5*, 992–996. [CrossRef]
18. Christensen, J.H.; Kanikicharla, K.K.; Aldrian, E.; An, S.I.; Cavalcanti, I.F.A.; de Castro, M.; Dong, W.; Goswami, P.; Hall, A.; Kanyanga, J.K.; et al. Climate phenomena and their relevance for future regional climate change. In *Climate Change 2013 the Physical Science Basis: Working Group I Contribution to the Fifth Assessment Report of the Intergovernmental Panel on Climate Change*; Cambridge University Press: Cambridge, UK, 2013; pp. 1217–11308.
19. Walsh, K.J.; McBride, J.L.; Klotzbach, P.J.; Balachandran, S.; Camargo, S.J.; Holland, G.; Knutson, T.R.; Kossin, J.P.; Lee, T.C.; Sobel, A.; et al. Tropical cyclones and climate change. *Wiley Interdiscip. Rev. Clim. Chang.* **2016**, *7*, 65–89. [CrossRef]
20. Knutson, T.; Camargo, S.J.; Chan, J.C.; Emanuel, K.; Ho, C.H.; Kossin, J.; Mohapatra, M.; Satoh, M.; Sugi, M.; Walsh, K.; et al. Tropical cyclones and climate change assessment: Part II: Projected response to anthropogenic warming. *Bull. Am. Meteorol. Soc.* **2020**, *101*, E303–E322. [CrossRef]
21. Kohno, N.; Dube, S.K.; Entel, M.; Fakhruddin, S.H.M.; Greenslade, D.; Leroux, M.D.; Rhome, J.; Thuy, N.B. Recent progress in storm surge forecasting. *Trop. Cyclone Res. Rev.* **2018**, *7*, 128–139.
22. Winter, G.; Storlazzi, C.; Vitousek, S.; van Dongeren, A.; McCall, R.; Hoeke, R.; Skirving, W.; Marra, J.; Reyns, J.; Aucan, J.; et al. Steps to Develop Early Warning Systems and Future Scenarios of Storm Wave-Driven Flooding Along Coral Reef-Lined Coasts. *Front. Mar. Sci.* **2020**, *7*, 1–8. [CrossRef]
23. Zheng, L.; Weisberg, R.H. Modeling the west Florida coastal ocean by downscaling from the deep ocean, across the continental shelf and into the estuaries. *Ocean Model.* **2012**, *48*, 10–29. [CrossRef]
24. Kerr, P.C.; Martyr, R.C.; Donahue, A.S.; Hope, M.E.; Westerink, J.J.; Luettich, R.A., Jr.; Kennedy, A.B.; Dietrich, J.C.; Dawson, C.; Westerink, H.J. US IOOS coastal and ocean modeling testbed: Evaluation of tide, wave, and hurricane surge response sensitivities to mesh resolution and friction in the Gulf of Mexico. *J. Geophys. Res. Ocean.* **2013**, *118*, 4633–4661. [CrossRef]
25. Kennedy, A.B.; Westerink, J.J.; Smith, J.M.; Hope, M.E.; Hartman, M.; Taflanidis, A.A.; Tanaka, S.; Westerink, H.; Cheung, K.F.; Smith, T.; et al. Tropical cyclone inundation potential on the Hawaiian Islands of Oahu and Kauai. *Ocean Model.* **2012**, *52*, 54–68. [CrossRef]
26. Hoeke, R.K.; McInnes, K.L.; O'Grady, J.; Lipkin, F.; Colberg, F. High Resolution Met-Ocean Modelling for Storm Surge Risk Analysis in Apia, Samoa. In *CAWCR Technical Report. 071*; The Centre for Australian Weather and Climate Research: Melbourne, Australia, 2014. Available online: https://www.cawcr.gov.au/technical-reports/CTR_071.pdf (accessed on 20 June 2021).
27. Joyce, B.R.; Gonzalez-Lopez, J.; Van der Westhuysen, A.J.; Yang, D.; Pringle, W.J.; Westerink, J.J.; Cox, A.T. US IOOS coastal and ocean modeling testbed: Hurricane-induced winds, waves, and surge for deep ocean, reef-fringed islands in the Caribbean. *J. Geophys. Res. Ocean.* **2019**, *124*, 2876–2907. [CrossRef]
28. Luettich, R.A.; Westerink, J.J.; Scheffner, N.W. ADCIRC: An advanced three-dimensional circulation model for shelves, coasts, and estuaries. Report 1. In *Theory and Methodology of ADCIRC-2DDI and ADCIRC-3DL*; Coastal Engineering Research Center: Vicksburg, MS, USA, 1992.
29. Booij, N.; Holthuijsen, L.H.; Ris, R.C. The "SWAN" wave model for shallow water. *Coast. Eng. Proc.* **1996**, *1*, 668–676.
30. Fleming, J.G.; Fulcher, C.W.; Luettich, R.A.; Estrade, B.D.; Allen, G.D.; Winer, H.S. A Real Time Storm Surge Forecasting System using ADCIRC. In Proceedings of the 10th International Conference on Estuarine and Coastal Modeling, Reston, VA, USA, 5–7 November 2007; pp. 893–912.
31. Dietrich, J.C.; Tanaka, S.; Westerink, J.J.; Dawson, C.N.; Luettich, R.A.; Zijlema, M.; Holthuijsen, L.H.; Smith, J.M.; Westerink, L.G.; Westerink, H.J. Performance of the unstructured-mesh, SWAN ADCIRC model in computing hurricane waves and surge. *J. Sci. Comput.* **2012**, *52*, 468–497. [CrossRef]

32. Ferreira, C.M.; Irish, J.L.; Olivera, F. Uncertainty in hurricane surge simulation due to land cover specification. *J. Geophys. Res. Ocean.* **2014**, *119*, 1812–1827. [CrossRef]
33. Deb, M.; Ferreira, C.M. Potential impacts of the Sunderban mangrove degradation on future coastal flooding in Bangladesh. *J. Hydro-Environ. Res.* **2017**, *17*, 30–46. [CrossRef]
34. Dietrich, J.C.; Bunya, S.; Westerink, J.J.; Ebersole, B.A.; Smith, J.M.; Atkinson, J.H.; Jensen, R.; Resio, D.T.; Luettich, R.A.; Dawson, C.; et al. A high-resolution coupled riverine flow, tide, wind, wind wave, and storm surge model for southern Louisiana and Mississippi. Part II: Synoptic description and analysis of Hurricanes Katrina and Rita. *Mon. Weather Rev.* **2010**, *138*, 378–404. [CrossRef]
35. Reddy, M.S.D. TROPICAL CYCLONE 'ISAAC', 28 FEBRUARY-3 MARCH 1982. *Weather Clim.* **1983**, *3*, 32–35. [CrossRef]
36. Hoeke, R.K.; McInnes, K.L.; Kruger, J.C.; McNaught, R.J.; Hunter, J.R.; Smithers, S.G. Widespread Inundation of Pacific Islands Triggered by Distant-Source Wind-Waves. *Glob. Planet. Chang.* **2013**, *108*, 128–138. [CrossRef]
37. McInnes, K.L.; Walsh, K.J.; Hoeke, R.K.; O'Grady, J.G.; Colberg, F.; Hubbert, G.D. Quantifying storm tide risk in Fiji due to climate variability and change. *Glob. Planet. Chang.* **2014**, *116*, 115–129. [CrossRef]
38. Mattocks, C.; Forbes, C. A real-time, event-triggered storm surge forecasting system for the state of North Carolina. *Ocean Model.* **2008**, *25*, 95–119. [CrossRef]
39. Lakshmi, D.D.; Murty, P.; Bhaskaran, P.K.; Sahoo, B.; Kumar, T.S.; Shenoi, S.; Srikanth, A. Performance of WRF-ARW winds on computed storm surge using hydrodynamic model for Phailin and Hudhud Cyclones. *Ocean Eng.* **2017**, *131*, 135–148. [CrossRef]
40. Ao, J.C.; Muhammad, A.; Curcic, M.; Fathi, A.; Dawson, C.N.; Chen, S.S.; Luettich, R.A., Jr. Sensitivity of storm surge predictions to atmospheric forcing during Hurricane Isaac. *J. Waterw. Port Coast. Ocean Eng.* **2018**, *144*, 04017035.
41. Holland, R.W. An analytic model of the wind and pressure profiles in hurricanes. *Mon. Weather Rev.* **1980**, *108*, 1212–1218. [CrossRef]
42. Gao, J. On the Surface wind Stress for Storm Surge Modeling. Doctoral Dissertation, The University of North Carolina at Chapel Hill, Chapel Hill, NC, USA, 2018.
43. Ramos Valle, A.N.; Curchitser, E.N.; Bruyere, C.L.; Fossell, K.R. Simulating storm surge impacts with a coupled atmosphere-inundation model with varying meteorological forcing. *J. Mar. Sci. Eng.* **2018**, *6*, 35. [CrossRef]
44. Powell, M.D.; Murillo, S.; Dodge, P.; Uhlhorn, E.; Gamache, J.; Cardone, V.; Cox, A.; Otero, S.; Carrasco, N.; Annane, B.; et al. Reconstruction of Hurricane Katrina's wind fields for storm surge and wave hindcasting. *Ocean. Eng.* **2010**, *37*, 26–36. [CrossRef]
45. Yin, J.; Lin, N.; Yu, D.P. Coupled modeling of storm surge and coastal inundation: A case study in New York city during hurricane sandy. *Water Resour. Res.* **2016**, *52*, 8685–8699. [CrossRef]
46. Velissariou, P.; Moghimi, S. *Parametric Hurricane Modeling System (PaHM) Manual*; NOAA: Washington, DC, USA, 2022.
47. Reardon, G.F.; Oliver, J. *Report on Damage Caused by Cyclone Isaac in Tonga*; Department of Civil & Systems Engineering, James Cook University: Townsville, Australia, 1982.
48. Mimura, N.; Pelesikoti, N. Vulnerability of Tonga to future sea-level rise. *J. Coast. Res.* **1997**, *24*, 117–132. Available online: http://www.jstor.org/stable/25736091 (accessed on 30 July 2022).
49. Department of Foreign Affairs and Trade. Crisis Hub-TC Harold. 2020. Available online: https://www.dfat.gov.au/crisis-hub/tropical-cyclone-harold (accessed on 25 May 2023).
50. Tonga Meteorological Service. *Meteorological Report on Severe Tropical Cyclone "Harold" (Category 4) 7th–9th April 2020*; Nuku'alofa, Tonga, 2020. Available online: https://met.gov.to/wp-content/uploads/2021/11/TC_HAROLD-REPORT.pdf (accessed on 30 June 2022).
51. Cylone Harold. 2020. Available online: https://en.wikipedia.org/wiki/Cyclone_Harold#:~:text=On%20April%2023%2C%20Tonga\T1\textquoterights%20Minister,excess%20of%20US%24111%20million (accessed on 20 April 2022).
52. Merrifield, M.A.; Becker, J.M.; Ford, M.; Yao, Y. Observations and estimates of wave-driven water level extremes at the Marshall Islands. *Geophys. Res. Lett.* **2014**, *41*, 7245–7253. [CrossRef]
53. Wandres, M.; Aucan, J.; Espejo, A.; Jackson, N.; De Ramon N'Yeurt, A.; Damlamian, H. Distant-source swells cause coastal inundation on Fiji's Coral Coast. *Front. Mar. Sci.* **2020**, *7*, 546. [CrossRef]
54. Hoeke, R.K.; Damlamian, H.; Aucan, J.; Wandres, M. Severe flooding in the atoll nations of Tuvalu and Kiribati triggered by a distant tropical cyclone pam. *Front. Mar. Sci.* **2021**, *7*, 539646. [CrossRef]
55. Tu'uholoaki, M.; Singh, A.; Espejo, A.; Chand, S.; Damlamian, H. Tropical cyclone climatology, variability, and trends in the Tonga region, Southwest Pacific. *Weather Clim. Extrem.* **2022**, *37*, 100483. [CrossRef]
56. Roelvink, D.; Reniers, A.; van Dongeren, A.; van Thiel de Vries, J.; McCall, R.; Lescinski, J. Modelling storm impacts on beaches, dunes and barrier islands. *Coast. Eng.* **2009**, *56*, 1133–1152. [CrossRef]
57. Luick, J.L.; Henry, R.F. Tides in the Tongan region of the pacific ocean. *Mar. Geod.* **2000**, *23*, 17–29. [CrossRef]
58. Bosserelle, C.; Reddy, S.; Lal, D. *Waves and Coast in the Pacific (WACOP) Wave Climate Reports*; Pacific Community: Suva, Fiji, 2015.
59. Stephens, S.A.; Ramsay, D.L. Extreme cyclone wave climate in the Southwest Pacific Ocean: Influence of the El Niño Southern Oscillation and projected climate change. *Glob. Planet. Chang.* **2014**, *123*, 13–26. [CrossRef]
60. Knapp, K.R.; Diamond, H.J.; Kossin, J.P.; Kruk, M.C.; Schreck, C.J. *International Best Track Archive for Climate Stewardship (IBTrACS) Project, Version 4. [Indicate Subset Used]*; NOAA National Centers for Environmental Information: Kiln, MS, USA, 2018. [CrossRef]
61. Diamond, H.J.; Lorrey, A.M.; Knapp, K.R.; Levinson, D.H. Development of an enhanced tropical cyclone tracks database for the southwest Pacific from 1840 to 2010. *Int. J. Climatol.* **2012**, *32*, 2240–2250. [CrossRef]

62. Roberts, K.J.; Pringle, W.J.; Westerink, J.J. OceanMesh2D 1.0: MATLAB-based software for two-dimensional unstructured mesh generation in coastal ocean modeling. *Geosci. Model Dev.* **2019**, *12*, 1847–1868. [CrossRef]
63. Tozer, B.; Sandwell, D.T.; Smith, W.H.F.; Olson, C.; Beale, J.R.; Wessel, P. Global Bathymetry and Topography at 15 Arc Sec: SRTM15+. *Earth Space Sci.* **2019**, *6*, 1847–1864. [CrossRef]
64. Aydoğan, B.; Ayat, B. Performance evaluation of SWAN ST6 physics forced by ERA5 wind fields for wave prediction in an enclosed basin. *Ocean. Eng.* **2021**, *240*, 109936. [CrossRef]
65. Rogers, W.E.; Hwang, P.A.; Wang, D.W. Investigation of wave growth and decay in the SWAN model: Three regional-scale applications. *J. Phys. Oceanogr.* **2003**, *33*, 366–389. [CrossRef]
66. Nelson, R.C. Depth limited design wave heights in very flat regions. *Coast. Eng.* **1994**, *23*, 43–59. [CrossRef]
67. Madsen, O.S.; Rosengaus, M.M. Spectral wave attenuation by bottom friction: Experiments. In *Coastal Engineering*; American Society of Civil Engineers: Reston, VA, USA, 1988; pp. 849–857.
68. Hasselmann, K.; Barnett, T.P.; Bouws, E.; Carlson, H.; Cartwright, D.E.; Enke, K.; Ewing, J.A.; Gienapp, A.; Hasselmann, D.E.; Kruseman, P.; et al. Measurements of wind-wave growth and swell decay during the Joint North Sea Wave Project (JONSWAP). *Ergaenzungsheft Zur Dtsch. Hydrogr. Z. Reihe A* **1973**. Available online: http://resolver.tudelft.nl/uuid:f204e188-13b9-49d8-a6dc-4fb7c20562fc (accessed on 19 July 2022).
69. Garratt, J.R. Review of drag coefficients over oceans and continents. *Mon. Weather Rev.* **1977**, *105*, 915–929. [CrossRef]
70. Lashley, C.H.; Roelvink, D.; van Dongeren, A.; Buckley, M.L.; Lowe, R.J. Nonhydrostatic and surfbeat model predictions of extreme wave run-up in fringing reef environments. *Coast. Eng.* **2018**, *137*, 11–27. [CrossRef]
71. Ford, M.; Merrifield, M.A.; Becker, J.M. Inundation of a low-lying urban atoll island: Majuro, Marshall Islands. *Nat. Hazards* **2018**, *91*, 1273–1297. [CrossRef]
72. Funakoshi, Y.; Hagen, S.C.; Bacopoulos, P. Coupling of hydrody- namic and wave models: Case study for Hurricane Floyd (1999) hindcast. *ASCE J. Waterw. Port Coast. Ocean Eng* **2008**, *134*, 321–335. [CrossRef]
73. Cyclone Harold. 2020. Available online: https://matangitonga.to/2020/04/15/satellite-tc-harold (accessed on 6 April 2023).
74. Akbar, M.K.; Kanjanda, S.; Musinguzi, A. Effect of Bottom Friction, Wind Drag Coefficient, and Meteorological Forcing in Hindcast of Hurricane Rita Storm Surge Using SWAN + ADCIRC Model. *J. Mar. Sci. Eng.* **2017**, *5*, 38. [CrossRef]
75. Camus, P.; Mendez, F.J.; Medina, R. A hybrid efficient method to downscale wave climate to coastal areas. *Coast. Eng.* **2011**, *58*, 851–862. [CrossRef]
76. Rueda, A.; Cagigal, L.; Pearson, S.; Antolínez, J.A.; Storlazzi, C.; van Dongeren, A.; Camus, P.; Mendez, F.J. HyCReWW: A hybrid coral reef wave and water level metamodel. *Comput. Geosci.* **2019**, *127*, 85–90. [CrossRef]
77. van Vloten, S.O.; Cagigal, L.; Rueda, A.; Ripoll, N.; Méndez, F.J. HyTCWaves: A Hybrid model for downscaling Tropical Cyclone induced extreme Waves climate. *Ocean Model.* **2022**, *178*, 102100. [CrossRef]